Draft version September 29, 2014
Preprint typeset using LaTeX style emulateapj v. 08/22/09

arXiv:1404.5335v2 [astro-ph.SR] 25 Sep 2014

A STATISTICAL ANALYSIS OF SEEDS AND OTHER HIGH-CONTRAST EXOPLANET SURVEYS: MASSIVE PLANETS OR LOW-MASS BROWN DWARFS?

Timothy D. Brandt[1], Michael W. McElwain[2], Edwin L. Turner[3,4], Kyle Mede[5], David S. Spiegel[1], Masayuki Kuzuhara[6,7,5], Joshua E. Schlieder[8], John P. Wisniewski[9], L. Abe[10], B. Biller[11], W. Brandner[8], J. Carson[12], T. Currie[13], S. Egner[14], M. Feldt[8], T. Golota[14], M. Goto[15], C. A. Grady[2], O. Guyon[14], J. Hashimoto[6], Y. Hayano[14], M. Hayashi[6], S. Hayashi[14], T. Henning[8], K. W. Hodapp[16], S. Inutsuka[17], M. Ishii[14], M. Iye[6], M. Janson[18], R. Kandori[6], G. R. Knapp[3], T. Kudo[6], N. Kusakabe[6], J. Kwon[6,19], T. Matsuo[6], S. Miyama[20], J.-I. Morino[6], A. Moro-Martín[21], T. Nishimura[14], T.-S. Pyo[14], E. Serabyn[22], H. Suto[6], R. Suzuki[6], M. Takami[23], N. Takato[14], H. Terada[14], C. Thalmann[24], D. Tomono[14], M. Watanabe[25], T. Yamada[26], H. Takami[14], T. Usuda[14], M. Tamura[5,6]

Draft version September 29, 2014

ABSTRACT

We conduct a statistical analysis of a combined sample of direct imaging data, totalling nearly 250 stars. The stars cover a wide range of ages and spectral types, and include five detections (κ And b, two $\sim$60 M_J brown dwarf companions in the Pleiades, PZ Tel B, and CD$-$35 2722B). For some analyses we add a currently unpublished set of SEEDS observations, including the detections GJ 504b and GJ 758B. We conduct a uniform, Bayesian analysis of all stellar ages using both membership in a kinematic moving group and activity/rotation age indicators. We then present a new statistical method for computing the likelihood of a substellar distribution function. By performing most of the integrals analytically, we achieve an enormous speedup over brute-force Monte Carlo. We use this method to place upper limits on the maximum semimajor axis of the distribution function derived from radial-velocity planets, finding model-dependent values of $\sim$30–100 AU. Finally, we model the entire substellar sample, from massive brown dwarfs to a theoretically motivated cutoff at $\sim$5 $M_{\rm Jup}$, with a single power law distribution. We find that $p(M,a) \propto M^{-0.65\pm0.60}a^{-0.85\pm0.39}$ (1σ errors) provides an adequate fit to our data, with 1.0–3.1% (68% confidence) of stars hosting 5–70 $M_{\rm Jup}$ companions between 10 and 100 AU. This suggests that many of the directly imaged exoplanets known, including most (if not all) of the low-mass companions in our sample, formed by fragmentation in a cloud or disk, and represent the low-mass tail of the brown dwarfs.

Subject headings:

1. INTRODUCTION

Since the first exoplanet around a main-sequence star was discovered in 1995 (Mayor & Queloz 1995), large radial velocity (e.g. Cumming et al. 2008; Bonfils et al. 2013) and transit surveys (Bakos et al. 2004; Pollacco et al. 2006; Batalha et al. 2013) have found many hundreds of worlds. Previous models of planet formation, extending back decades (e.g. Kuiper 1951; Hayashi 1981), were based heavily on the Solar system. New discoveries have enabled a much fuller characterization of exoplanets within $\sim$3 AU of their host stars, around both main sequence (Cumming et al. 2008) and evolved (Johnson et al. 2007b) systems. These distributions hold clues to the formation and subsequent dynamical evolution of planetary systems.

While constraints on the mass function of planets have only recently been determined, the initial mass function (IMF) of stars has been studied for many decades (Salpeter 1955), and is now well-constrained. The stellar IMF has also recently been extended to brown dwarfs (Kroupa 2001; Reid et al. 2002; Chabrier 2003), objects below the minimum mass ($\sim$80 M_J) necessary to sustain hydrogen fusion, but above the minimum mass for deuterium burning ($\sim$13 M_J). Large samples of sub-

* Based on data collected at Subaru Telescope, which is operated by the National Astronomical Observatory of Japan
[1] Institute for Advanced Study, Princeton, NJ, USA
[2] Exoplanets and Stellar Astrophysics Laboratory, Goddard Space Flight Center, Greenbelt, MD, USA
[3] Department of Astrophysical Sciences, Princeton University, Princeton, NJ, USA
[4] Kavli Institute for the Physics and Mathematics of the Universe (WPI), Todai Institutes for Advanced Study, University of Tokyo, Tokyo, Japan
[5] University of Tokyo, Tokyo, Japan
[6] National Astronomical Observatory of Japan, Tokyo, Japan
[7] Tokyo Institute of Technology, Tokyo, Japan
[8] Max Planck Institute for Astronomy, Heidelberg, Germany
[9] HL Dodge Department of Physics and Astronomy, University of Oklahoma, Norman, OK, USA
[10] Laboratoire Hippolyte Fizeau, Nice, France
[11] University of Edinburgh, Edinburgh, Scotland, UK
[12] College of Charleston, Charleston, SC, USA
[13] Department of Astronomy and Astrophysics, University of Toronto, Toronto, ON, Canada
[14] Subaru Telescope, Hilo, Hawai'i, USA
[15] Universitäts-Sternwarte München, Munich, Germany
[16] Institute for Astronomy, University of Hawai'i, Hilo, Hawai'i, USA
[17] Department of Physics, Nagoya University, Nagoya, Japan
[18] Queens University Belfast, Belfast, Northern Ireland, UKt
[19] Department of Astronomical Science, Graduate University for Advanced Studies, Tokyo, Japan
[20] Hiroshima University, Higashi-Hiroshima, Japan
[21] Space Telescope Science Institute, Baltimore, MD, USA
[22] Jet Propulsion Laboratory, California Institute of Technology, Pasadena, CA, USA
[23] Institute of Astronomy and Astrophysics, Academia Sinica, Taipei, Taiwan
[24] Institute for Astronomy, ETH Zürich, Zürich, Switzerland
[25] Department of Cosmosciences, Hokkaido University, Sapporo, Japan
[26] Astronomical Institute, Tohoku University, Sendai, Japan

stellar objects are difficult to assemble, both because brown dwarfs have a limited supply of internal energy, and because the IMF turns over near the hydrogen-burning boundary. Brown dwarfs are also uncommon as close companions to main-sequence stars, a phenomenon known as the "brown dwarf desert" (Marcy & Butler 2000; Grether & Lineweaver 2006). The companion mass function (CMF) rises from this "desert" both towards higher, stellar masses, and towards lower, planetary masses.

The companion mass function, well-established at small separations from radial velocity surveys (Cumming et al. 2008), is much less clear at tens of AU. The conditions in a protoplanetary disk are very different far from the host star and may not support the formation mechanism responsible for the radial-velocity (RV) distribution (Dodson-Robinson et al. 2009), though such a conclusion is far from certain (Lambrechts & Johansen 2012; Kenyon & Bromley 2009). Companions near or below the deuterium-burning limit might form like stars in gravitational collapse or fragmentation (Boss 1997; Vorobyov 2013), by core-accretion in-situ (Pollack et al. 1996; Alibert et al. 2005), or they might form in a location more conducive to planet formation and subsequently migrate or be scattered to their observed orbits. The distribution function of such objects could provide important clues to their formation mechanism, and connect them to either more massive brown dwarfs or to the planet populations observed at smaller separations. As a result, these massive exoplanets are being heavily targeted using large telescopes with adaptive optics.

The sensitivity to exoplanets with direct imaging has been rapidly improving, and recent discoveries have begun to fill the parameter space of substellar objects at separations of tens of AU. Companions near or below the deuterium burning limit have been discovered around the M-dwarfs 2MASS J01225093-2439505 (Bowler et al. 2013), 2MASS J01033563-5515561AB (Delorme et al. 2013), and ROXs 42B (Currie et al. 2014), the G-dwarf GJ 504 (Kuzuhara et al. 2013), the A stars HR 8799 (Marois et al. 2008, 2010), β Pictoris (Lagrange et al. 2009), and HD 95086 (Rameau et al. 2013), and the late B star κ And (Carson et al. 2013). These detections were made possible by recent technological advances in adaptive optics and the use of differential imaging techniques. In addition, recent work to identify nearby members of young moving groups (MGs, e.g. Torres et al. 2008; Zuckerman et al. 2011; Schlieder et al. 2012; Shkolnik et al. 2012; Malo et al. 2013; Moór et al. 2013; Rodriguez et al. 2013; Gagné et al. 2014) and stars that harbor debris disks (Rieke et al. 2005; Chen et al. 2006; Plavchan et al. 2009; Moór et al. 2011; Eiroa et al. 2011) has provided excellent targets for direct imaging searches. The stellar age is particularly important, because substellar objects are unable to sustain hydrogen fusion in their cores, and quickly fade beneath the sensitivity limits of the best observing facilities on the ground and in space.

Over the last decade, numerous direct imaging surveys around nearby young stars have begun to constrain the distribution and frequency of substellar companions. These have mostly used non-detections to place upper limits on the planet fraction within a range of masses and semimajor axes, or upper limits beyond which the distribution function measured by radial velocity surveys cannot extend. Lafrenière et al. (2007) used the Gemini Deep Planet Survey (GDPS) to place upper limits of $\sim$10% on the fraction of stars with 0.5–13 M_J companions in the range from 50 to 250 AU, assuming an RV-like mass distribution. Nielsen & Close (2010) used a sample of 118 targets, dominated by the GDPS, to find that the RV distribution of Cumming et al. (2008) cannot be extrapolated past $a_{\rm max}$ from $\sim$65–200 AU depending on the substellar cooling model and on the correlation between planet frequency and stellar mass. Chauvin et al. (2010) imaged 88 stars, around which they detected three substellar companions, including an $\sim$8-M_J companion to the brown dwarf 2M1207 and a $\sim$13 M_J companion to AB Pic. More recently, Vigan et al. (2012) placed a lower limit to the planet ($<$13-M_J) frequency around A stars of 6% based on the International Deep Planet Survey and the detections around HR 8799 and β Pictoris. Biller et al. (2013) placed a similar model-dependent upper limit of 6%–18% for companions from 1–20 M_J between 10 and 150 AU around later-type stars. Chauvin et al. (2014) observed 86 stars without detecting substellar companions, placing an upper limit of 10% on 5–10 $M_{\rm Jup}$ objects 50–500 AU from young solar-type stars. However, the distribution function for these companions remains uncertain, and statistical analyses often artificially truncate it at or near the deuterium burning threshold.

In this work, we provide a new framework for determining the distribution function of substellar companions to stars, and apply this framework to the published sub-sample of the Subaru SEEDS survey, combined with the publicly available GDPS (Lafrenière et al. 2007) and NICI MG sample (Biller et al. 2013). In Section 2, we discuss what is currently known about the stellar and substellar mass distributions. In Section 3, we present our combined data set, and in Section 4, we summarize our method for deriving their age probability distributions; in Section 5, we discuss our choice of substellar cooling models. We present our statistical framework and method for determining constraints on the substellar distribution function in Section 6, with additional details, derivations, and fitting functions in the Appendix. Section 7 presents and discusses our results, including our limits on an extrapolated RV-like distribution function, and the ability of a single distribution to include most or all wide-separation substellar objects. We conclude with Section 8.

2. A TAIL OF TWO DISTRIBUTIONS

In spite of their rarity, brown dwarf and very massive ($\gtrsim$10 $M_{\rm Jup}$) giant planet companions are now being discovered at wide separations around nearby stars, both by dedicated high-contrast surveys and by mid-infrared space missions such as the *Wide-field Infrared Survey Explorer* (*WISE*). In contrast, less-massive exoplanets at wide separations remain extremely scarce: only two known companions to stellar primaries are likely to have masses less than 5 $M_{\rm Jup}$: GJ 504b (Kuzuhara et al. 2013), and HD 95086b (Rameau et al. 2013). LkCa 15b (Kraus & Ireland 2012) and, especially, Fomalhaut b (Kalas et al. 2008; Janson et al. 2012; Currie et al. 2012) may also fall into this category, though their natures remain unclear. The paucity of known $\sim$3–5 M_J companions might indicate a lack of planets rather than simply

our inability to detect them. High-contrast surveys have now observed ∼1000 nearby stars, often with sensitivities to objects significantly less massive than those detected around β Pictoris and HR 8799 at moderate to wide separations ($\gtrsim 1''$).

The mass distribution function of short-period companions, as determined by radial velocity surveys, is now well-determined. It decreases sharply from ∼1 M_J to ∼20 M_J, then increases towards stellar masses (Marcy & Butler 2000; Grether & Lineweaver 2006). Cumming et al. (2008), using eight years of radial velocity data and assuming $dN/dM \propto M^{\beta}$, find $\beta_{\rm pl} = -1.31 \pm 0.2$ for $M_{\rm pl} > 0.3$ M_J and periods <2000 days. The relative lack of companions in the mass range from ∼10 M_J to ∼40 M_J is known as the brown dwarf desert. This "desert," however, is significantly less pronounced at wider separations (Gizis et al. 2001; Metchev & Hillenbrand 2009).

Recent discoveries have illuminated the brown dwarf mass function in the field, favoring a power law index $\beta_{\rm BD} \sim 0$ for a mass distribution of the form $dN/dM \propto M^{\beta}$. The mass distribution is certainly not an extension of that of low-mass stars (Kroupa 2001; Reid et al. 2002; Chabrier 2003), and the best-fitting piecewise power law may be discontinuous (Thies & Kroupa 2007). Thies & Kroupa (2008) find a best fit $\beta_{\rm BD} \sim -0.3$ using young clusters, while Kirkpatrick et al. (2012) find $0 \lesssim \beta_{\rm BD} \lesssim 0.5$ in the very nearby field, and Sumi et al. (2011) report $\beta_{\rm BD} = -0.49^{+0.27}_{-0.24}$ based on gravitational microlensing events. Sumi et al. (2011) hypothesized a distribution of low-mass "rogue planets" in the field to explain their shortest duration microlensing events, and found $\beta = -1.3^{+0.4}_{-0.3}$ for such a population, consistent with that found for radial velocity companions. A value $\beta_{\rm BD} = 0$ corresponds to equal numbers of objects at all brown dwarf masses, with most of the matter residing in massive objects.

The brown dwarf mass function in binaries is more controversial. Metchev & Hillenbrand (2009), in a high-contrast imaging survey of young stars, found their data to be consistent with a single power law companion mass function with $\beta \approx -0.4$ extending all the way from 1 $M_\odot$ down to the deuterium-burning limit of ∼13 M_J. This result is strongly inconsistent with the distribution of companion masses seen at small separations. In contrast, Zuckerman & Song (2009) derived the brown dwarf companion mass function from a survey of objects reported in the literature, and found a much steeper $\beta \sim -1.2$. However, hydrodynamical simulations disfavor such a strong peak at low masses, with Stamatellos & Whitworth (2009) finding a relatively flat distribution of cloud fragment masses over the brown dwarf regime.

As with the mass distribution, the semimajor axis distributions for stellar binaries and for close ($\lesssim$3 AU) exoplanets are both well-determined. Cumming et al. (2008) find $\alpha = -0.61 \pm 0.15$ for $dN/da \propto a^{\alpha}$ in the range from 0.03–3 AU, i.e., a distribution with planet incidence decreasing with separation, but still divergent if integrated to infinity. The semimajor axis distribution of companions to G-dwarfs is approximately log-normal, with a peak in the distribution at ∼30–50 AU for a star of 1 $M_\odot$ (Duquennoy & Mayor 1991; Raghavan et al. 2010). In the range $5 < a < 500$ AU, the space most relevant to high-contrast imaging, the observed distribution is very nearly flat in $\log a$ (varying by ∼30%).

The mass (and separation) ranges over which the planet and brown dwarf distributions apply are controversial. The IAU draft definition of a planet is simply any object which is both bound to a star and below the minimum mass for deuterium burning, currently calculated to be ∼13 M_J (Spiegel et al. 2011). However, this criterion holds no other physical significance and is independent of the object's formation mechanism. Brown dwarfs are thought to form like stars, and, though the minimum fragment mass is not known precisely, it is likely to fall at around 5 M_J (Low & Lynden-Bell 1976; Bate et al. 2003; Bate 2009). Some studies (Bate et al. 2003; Umbreit et al. 2005) suggest that brown dwarfs form when they are ejected from dynamically unstable systems, making it extremely difficult to form substellar companions to solar-type stars by cloud fragmentation. However, in the outer regions of a disk rather than in a molecular cloud, fragmentation may be more likely to produce substellar objects (Boss 1997), though the lower mass cutoff is still likely to be several M_J (Rafikov 2005; Whitworth & Stamatellos 2006).

Substellar objects near or below the deuterium burning limit of ∼13 M_J have been discovered at separations from ∼40 AU to ∼1000 AU around stars ranging in spectral type from late M to late B (e.g. Chauvin et al. 2005b; Marois et al. 2008; Lagrange et al. 2009; Bowler et al. 2013; Carson et al. 2013; Currie et al. 2014). Two recent discoveries, GJ 504b (Kuzuhara et al. 2013) and HD 95086b (Rameau et al. 2013), plus HR 8799b (Sudol & Haghighipour 2012), push the mass range of such companions down to ∼5 M_J. If these objects could form by core-accretion (Pollack et al. 1996; Alibert et al. 2005; Lambrechts & Johansen 2012), believed to be responsible for gas giants at smaller separations, they might be an extension of the radial velocity distribution (nearly all planets of which, presumably, formed via core accretion). If, however, they form by fragmentation in a cloud or disk (e.g. Boss 1997; Vorobyov 2013), they should be considered together with low-mass brown dwarfs, and perhaps with the entire substellar distribution up to a mass of ∼0.1 $M_\odot$, where the initial mass function turns over and starts rising toward higher mass. It is also possible that more than one of these distributions overlap in parameter space, and that the sample of direct-imaging discoveries is a heterogeneous population with multiple modes of formation (Boley 2009).

Because many discoveries straddle the deuterium burning threshold (depending on the assumed age of the system and on the substellar cooling model), and because there is no theoretical motivation to separate objects at 13 M_J, we consider giant planets and low-mass brown dwarfs together. It is certainly possible that the most massive brown dwarfs ($\gtrsim$50 M_J) are drawn from a different distribution, but we see no reason to impose such a division *à priori*, particularly not at 13 M_J. The form of the distribution function and its limits in mass and semimajor axis should be powerful clues to the formation mechanism at work. We note, however, that we are still limited by our reliance on uncertain models of substellar cooling and by our parametrization of the distribution function with limited theoretical motivation.

3. HIGH CONTRAST IMAGING DATA SET

We merge five samples to create our high-contrast data set: three published subgroups of the Strategic Exploration of Exoplanets and Disks with Subaru project (SEEDS, Tamura 2009), the Gemini Deep Planet Survey (GDPS, Lafrenière et al. 2007), and the MG targets from the NICI survey (Biller et al. 2013). We discuss each of these in turn. In total, our merged survey contains 248 unique stars with spectral types ranging from late B to mid M, at distances from ∼5 pc to ∼130 pc, with sensitivities down to ∼1 M_J around the nearest, youngest targets. We reduce most of the data, including that of GDPS targets but excepting the NICI stars, using ACORNS-ADI (Brandt et al. 2013); for GDPS stars, our results are very similar to those published in Lafrenière et al. (2007). For the NICI data, we use the published reductions as described by Wahhaj et al. (2013a).

After reviewing each of the five samples, we apply a uniform, Bayesian analysis to compute age probability distributions. This analysis combines proposed MG membership, rotation and activity indicators, all of which are listed in Table 1. We provide a summary in Section 4, with the full procedure described in Brandt et al. (2014). The secondary age indicators of the SEEDS MG sample are listed in Brandt et al. (2014), while the indicators for the other samples are listed in Table 1. Our age analysis also requires us to estimate the probability of MG membership for each target. Most of our targets are either consensus members of a MG (listed as 95%+ probability in Table 1) or consensus nonmembers, though a few are more uncertain. We briefly discuss each such case, including our adopted MG classification and membership probability, in Section 3.4.

In addition to the 248 stars in this sample, we consider two additional stars around which HiCIAO has detected substellar companions: GJ 758B (Thalmann et al. 2009; Janson et al. 2011), a ∼30 M_J brown dwarf around an old G star first imaged during HiCIAO commissioning, and GJ 504b (Kuzuhara et al. 2013; Janson et al. 2013a), a ∼3–8 M_J companion to an active field G star discovered during the full SEEDS survey. By using these discoveries in part of our statistical analysis, we assume that the stars and contrast curves of ∼200 as-yet-unpublished SEEDS targets are similar to those of the merged sample we discuss in this section. This is a fairly good approximation; in fact, the unpublished SEEDS targets are primarily a combination of relatively distant (∼100 pc), very young (∼5–10 Myr) pre-main-sequence stars, and very nearby stars (∼5–50 pc) with a wide range of ages (tens of Myr to several Gyr) and spectral types (A through M).

3.1. *SEEDS*

SEEDS (Tamura 2009) is now mostly complete, having observed nearly 400 nearby stars with the high-contrast camera HiCIAO (Suzuki et al. 2010) behind the 188-actuator adaptive optics system AO188 (Hayano et al. 2008). For this study, we use the previously published data sets comprised of debris disk hosts (Janson et al. 2013b), proposed members of nearby MGs (Brandt et al. 2014), and Pleiades members (Yamamoto et al. 2013). The Pleiades targets are young, with ages that are better-constrained than those of typical field stars.

The SEEDS MG sample is described in detail in Brandt et al. (2014). That work includes stellar age indicators and Bayesian age estimates for all targets, both those that are reliable members of coeval MGs and those that are not. We adopt those indicators and ages throughout the rest of this work. There is much less controversy over membership in the Pleiades, a rich, young (125 ± 8 Myr; Stauffer et al. 1998) stellar cluster at a distance of ∼130 pc. There is, however, considerable controversy over the distance to the Pleiades, with *Hipparcos* parallaxes favoring a value of 120 pc (van Leeuwen 2009), against isochrone fitting and other techniques giving a value about 10% larger (An et al. 2007; Munari et al. 2004). These differences are of marginal significance to our work. We adopt a distance of 130 ± 10 pc for all imaged Pleiades targets, together with a slightly more conservative age of 125 ± 10 Myr.

The MG sample includes one substellar detection, κ And b (Carson et al. 2013). The object lies at a projected separation of 55 AU, and has a mass of ∼13 M_J assuming the primary, κ And, to be a member of the ∼30-Myr Columba MG. Recent papers have called its Columba membership into question due to the star's position on the color-magnitude diagram, which hints at an age of several hundred Myr and a mass of ∼50 M_J for the companion (Hinkley et al. 2013; Bonnefoy et al. 2014). The Pleiades targets include two substellar detections: H II 1348B (Geißler et al. 2012) and HD 23514B (Rodriguez et al. 2012). H II 1348B and HD 23514B lie at projected separations of 140 and 310 AU respectively, and each has a mass of ∼60 M_J. Neither discovery was published when the SEEDS observations were made.

The debris disk sample has its stellar properties listed in Table 4 of Janson et al. (2013b). For this work, we revisit the ages using the Bayesian techniques presented in Brandt et al. (2014) and summarized in Section 4.

3.2. *GDPS*

GDPS (Lafrenière et al. 2007) used the NIRI instrument on Gemini-North to take high-contrast near-infrared images of 85 nearby stars. The stars ranged from F to M dwarfs, and were selected to be young, as inferred from their membership in kinematic MGs or from fits to color-magnitude isochrones. As for our other data sets, we generally do not consider isochrone ages. These are typically unreliable for main-sequence stars that have completed $\lesssim 1/3$ of their main-sequence lives (Soderblom 2010, and references therein), precisely those that we are most interested in dating. We do consider isochrones in some cases where a MG identification is in doubt (Brandt et al. 2014). GDPS did not detect any substellar companions to its targets, though the survey did find several new stellar binaries.

3.3. *NICI*

We also include the unique stars added by the southern sample observed by Biller et al. (2013) using the NICI instrument on Gemini-South. To enable a straightforward comparison to the data from the other surveys, we consider only those stars observed with angular differential imaging in the H-band, excluding those targets with spectral differential imaging (SDI). Biller et al. (2013) also report 95% completeness levels rather than 5σ (or 5.5 or 6σ) thresholds, where σ is the standard deviation of the background at a given separation. In order to

convert these levels into a common framework with the values reported by other surveys, we assume the residuals to be Gaussian (a very good approximation for SEEDS and GDPS). A 95% completeness threshold, assuming a 5σ minimum for follow-up, corresponds to a source bright enough to be detected if it were located on 95% of the background fluctuations. Given that a Gaussian distribution with zero mean has 95% of its probability above -1.64σ, a 6.64σ source would be detected at 5σ or better 95% of the time. We therefore convert the 95% limits to 5σ sensitivity curves by adding

$$2.5 \log_{10} \frac{6.64}{5} \approx 0.31 \text{ mag} , \quad (1)$$

and proceed to include the modified sensitivity curves in the remainder of our analysis. The NICI sample includes two substellar detections: a $\sim$35 M_J brown dwarf around HIP 92680 (= PZ Tel, Biller et al. 2010), and a $\sim$30 M_J brown dwarf around TYC 7084-794-1 (= CD−35 2722, Wahhaj et al. 2011). HD 1160 was not in the NICI MG sample, so its brown dwarf companion (Nielsen et al. 2012) does not enter our analysis.

3.4. *Targets with Uncertain MG Membership*

Most of the stars in our combined sample are either very high probability members of a given MG (95%+ in Table 1), or are unlikely to be members of any known MG. We generally consider a star to be an uncontroversial MG member if it has a 99% or higher membership probability as given by Malo et al. (2013), or a 95% or higher membership probability according to Gagné et al. (2014) (who updated Malo et al. to include non-uniform priors), together with at least one additional youth indicator. The Bayesian analyses of Malo et al. (2013) and Gagné et al. (2014) include position and proper motion and, where available, radial velocity and parallax (giving a position in six-dimensional phase space). Not all of the high probability members have radial velocity and parallax measurements (e.g. most TW Hydrae stars were too faint for *Hipparcos*), but a Bayesian analysis accounts for this.

This section summarizes the information for those stars which fall short of our criteria for near-certain MG membership, but are still possible or likely members of a MG. All stars in the following summary have position, proper motion, parallax, and radial velocity measurements unless otherwise noted.

3.4.1. *SEEDS Debris Disk Targets*

HIP 7345—Zuckerman & Song (2012) identify this early A star as a member of the Argus association, a classification definitively rejected by BANYAN-II[28] at 99% probability. We decline to identify the star with any association.

HIP 7576—This mid-G star was classified in the Hercules-Lyra association, which we consider to be unreliable for dating (Brandt et al. 2014). It does show abundant youth indicators, and its kinematics and parallax also fit very nicely with the predictions for β Pic membership; BANYAN places it in β Pic with over 99% probability. We provisionally adopt the β Pic classification here, though the secondary age indicators are slightly more consistent with an age of several hundred Myr, rather than the $\sim$20 Myr of β Pic.

HIP 11360—This early F star is listed as a bona-fide member with ambiguous group membership (Malo et al. 2013). Torres et al. (2006) suggest membership in β Pic, while Malo et al. (2013) find a better fit with membership in Columba; the BANYAN II analysis (without a radial velocity) also places a significant ($\sim$15%) probability of field membership. We provisionally adopt the Columba classification, with its slightly older age, at 85% probability.

HIP 11847—The BANYAN web tool lists a 99% probability of β Pic membership for this early F star (with radial velocity from Moór et al. 2011), though BANYAN II finds a probability of just $\sim$13%. Moór et al. (2011) also note a nearby star with similar space motions and strong youth indicators, supporting β Pic membership for both stars. HIP 11847 hosts a bright debris disk (Moór et al. 2011), and its isochrone-based age likelihood (see Brandt et al. 2014, for details) is consistent with an age from $\sim$20–200 Myr. For this work, we adopt a 50% probability of β Pic membership.

HIP 13402—BANYAN gives a $\sim$70% membership probability in β Pic for this early K star; BANYAN II gives 22%. It has abundant secondary age indicators, including vigorous X-ray and chromospheric activity, rapid rotation, and abundant lithium, all consistent with a very young age. We adopt the lower probability here.

HIP 57632—Zuckerman et al. (2011) classified this early A star as a member of the Argus association, which BANYAN II confirms, with a probability of just over 90%. We accept Argus membership with the latter's significance.

HIP 76829—This F4 star lacks any youth indicators apart from its kinematics, and has not been proposed as a bona fide member of any kinematic MG apart from the Hercules-Lyra association (López-Santiago et al. 2006), which we consider to be unreliable for dating (Brandt et al. 2014). The star is too massive to show strong magnetic activity. Its position on the color-magnitude diagram appears to be consistent with either an age of $\sim$20 Myr, consistent with β Pic, or several hundred Myr. For this analysis, we adopt BANYAN II's 84% membership probably in β Pic.

HIP 77542—This B9.5 star is a pre-main-sequence object with a relatively gas-rich disk (Merín et al. 2004), marking it as a very young object. We follow Merín et al. (2004) in adopting an age of 5 ± 1 Myr.

HIP 79977—This F2 star is a consensus member of the Upper Scorpuis OB association (de Zeeuw et al. 1999). We adopt an age of 11 ± 3 Myr for the association, consistent with two recent estimates (Pecaut et al. 2012; Song et al. 2012).

3.4.2. *non-SEEDS GDPS Targets*

HIP 9291—BANYAN II places this mid-M star in Carina with $\sim$75% probability. It does show vigorous X-ray activity and is rapidly rotating, with $v \sin i \sim 15$ km s^{-1} (Głębocki & Gnaciński 2005). Given these signs of youth, we provisionally accept the 75% probability estimate of Columba membership.

HIP 44458—This G0 star has very strong secondary

[28] See http://www.astro.umontreal.ca/~ malo/banyan.php, http://www.astro.umontreal.ca/~gagne/banyanII.php

youth indicators, including strong lithium absorption and rapid rotation. While BANYAN gives a 70% probability of membership in Columba, BANYAN II gives just 3%. We decline to identify the star with any MG, relying instead on its abundant secondary age indicators.

HIP 72339—BANYAN places this star in AB Dor with 96% probability based on its kinematics; BANYAN II gives a 24% probability of AB Dor membership. However, none of its youth indicators are consistent with such a young age; its lithium and activity levels are more consistent with an age of ∼1 Gyr. The isochrone-based likelihood shows two peaks, one around ∼50 Myr, and another around 1 Gyr. We therefore provisionally reject AB Dor membership.

HIP 105038—BANYAN places this K3 star in either Columba or β Pic with high probability based on its kinematics. However, its youth indicators favor a much older age, and BANYAN II places it in the field with over 90% probability. Similarly to HIP 72339, we provisionally reject Columba membership.

HIP 113020—This mid-M star, GJ 876, is known to host four planets discovered by radial velocity (Delfosse et al. 1998; Marcy et al. 1998, 2001; Rivera et al. 2005, 2010). It has only a very weak upper limit on X-ray activity and a measurement of slow rotation ($\sim$2 km s^{-1}, Głębocki & Gnaciński 2005) to corroborate BANYAN's 99.9% classification in β Pic (85% in BANYAN II). Marcy et al. (2001) estimate HIP 113020's age to be >1 Gyr due to its lack of activity, which would be exceptional in a ∼20 Myr-old β Pic member. We decline to identify the star with any moving group.

HIP 115147—This K1 star shows very strong chromospheric and X-ray activity, rapid rotation ($\sim$16 km s^{-1}, Głębocki & Gnaciński 2005), and retains abundant lithium, all consistent with a young age. We therefore accept BANYAN's 80% probability in Columba membership.

HIP 116215—While BANYAN II places this mid-K star in β Pic with 77% probability, it lacks any detectable lithium, and shows only moderately vigorous chromospheric and coronal activity. We consider its membership to be doubtful, and provisionally assign a 20% membership probability in β Pic.

3.4.3. *non-SEEDS, non-GDPS NICI MG ADI Targets*

HIP 9685—This star is a high probability (over 99% according to BANYAN II) member of Tuc-Hor neglecting a discrepant radial velocity. However, Biller et al. (2013) reported a ∼0.5 $M_\odot$ stellar companion at a projected separation of 0.″18 (9 AU), naturally explaining a 7–8 km s^{-1} shift in the radial velocity. We therefore regard HIP 9685 as a reliable member of Tuc-Hor.

TYC 5899-26-1—With a measured radial velocity (26.7 ± 1.5 km s^{-1} Schlieder et al. 2010) and parallax (61.4 ± 1.5 mas, Shkolnik et al. 2012), BANYAN II confirms AB Dor membership with 99.9% probability. This is consistent with the star's strong X-ray activity.

HIP 26373—BANYAN places this star in AB Dor with 100% probability, falling to 87% in BANYAN II. It shows a wide range of youth indicators consistent with an age of ∼100 Myr, including abundant lithium, rapid rotation, and saturated chromospheric and X-ray emission. We consider it to be a high-probability member of AB Dor.

TYC 5361-1476-1—da Silva et al. (2009) classified this star as a member of AB Dor, but BANYAN II places higher probability on its membership in β Pic (84% in β Pic; 3% in AB Dor, 13% in the field). The star does have strong youth indicators, including vigorous X-ray activity, rapid rotation, and abundant lithium, and is very likely to be young. Unfortunately, conclusive membership in a MG will require the measurement of a radial velocity and a parallax. For now, we adopt a 90% membership probability in AB Dor, effectively being conservative about its identification with β Pic (and the younger age this would imply).

TYC 7084-794-1 (= CD−35 2722)—While BANYAN II's membership probability of 85% is much lower than BANYAN's 99.9%, the star shows strong indicators of youth, and we consider it to be a reliable member of AB Dor. The star does have a measured radial velocity, but no parallax.

HIP 30034—Zuckerman & Song (2004) originally proposed this star to be a member of Tuc-Hor, though Torres et al. (2008) favor membership in Columba and Malo et al. (2013) favor membership in Carina. All of these associations are of similar age (∼30 Myr), making the distinction not particularly meaningful for our analysis. HIP 30034 does show strong youth indicators and is highly likely to be young; BANYAN and BANYAN II both strongly disfavors membership in the field. We adopt a 95+% membership probability in Carina, with the understanding that this probability encompasses HIP 30034's possible membership in Columba (or, less likely, in Tuc-Hor).

GSC 08894-00426—This M dwarf lacks a radial velocity or parallax, and is also almost fully depleted in lithium. BANYAN disfavors field membership, placing a 70% probability on β Pic membership, 12% in Argus, and 16% in AB Dor, while BANYAN II gives an 89% probability of β Pic membership and a 6% probability of AB Dor membership, with a 4% probability of membership in the field. Craig et al. (1997) list a spectral type of M5, which would make its lack of lithium somewhat surprising in the context of likely low-mass members of β Pic (Binks & Jeffries 2014); however, it is sufficiently close to the lithium depletion boundary to make a conclusive statement impossible. Unfortunately, a firm membership in any MG must await a radial velocity and parallax measurement. We provisionally (and conservatively) assign it to AB Dor, the oldest MG of which GSC 08894-00426 is a plausible member.

GJ 9251 A—Listed as a member of AB Dor by Biller et al. (2013), this star is conclusively associated with the field by BANYAN (>99% probability). In addition, it has only an upper limit on X-ray luminosity, and lacks any detected rotation period or chromospheric emission; López-Santiago et al. (2010) measure $v \sin i < 1$ km s^{-1}. We therefore reject the proposed MG association.

TYC 8728-2262-1—This star presents an extreme disagreement between the results using BANYAN, which gives a 99% probability of β Pic membership, and BANYAN II, which gives the probability as just 4%. The star is certainly young: it shows saturated X-ray emission, rapid rotation, and abundant lithium. Lacking a parallax, we adopt a 50% probably of β Pic membership.

TYC 9073-762-1—This star is another case of a strong disagreement between BANYAN (99.9% in β Pic) and

BANYAN II (67% in β Pic). As for TYC 8728-2262-1 above, the star shows abundant youth indicators but lacks a measured parallax. We adopt an 80% probability of β Pic membership.

TYC 7408-54-1—This star is similar to the two cases above, with nonuniform priors reducing BANYAN II's probability of β Pic membership from 99.9% to 60%. Due to its abundant youth indicators, we adopt an 80% membership probability. The measurement of a parallax will clear up each of these three cases.

HIP 95261—This A star is known to have a brown dwarf companion (Lowrance et al. 2000). Originally proposed as a member of TW Hya (Zuckerman & Webb 2000) but soon reclassified into β Pic (Zuckerman et al. 2001), BANYAN rejects membership in any MG due to a discrepant radial velocity. Malo et al. (2013) suggest that the radial velocity could be affected by the late-type companion, though a $\sim$0.2 $M_\odot$ companion 200 AU ($4''$ projected at 50 pc) from a $\sim$2 $M_\odot$ primary would induce a radial velocity of just a few tenths of a km s^{-1}, far too little to explain a $\sim$15 km s^{-1} discrepancy. Malo et al. also suggest that, with such a rapid rotator ($v \sin i = 330$ km s^{-1}, da Silva et al. 2009), the radial velocity could simply be in error. We acknowledge this as a possibility, but provisionally adopt a much lower β Pic membership probability of 50%.

2MASS J19560294-3207186 and TYC 7443-1102-1—These stars share a common proper motion, but lack a measured parallax. Kiss et al. (2011) have measured a radial velocity for TYC 7443-1102-1, resulting in a 99.8% membership probability in β Pic according to BANYAN, and 58% according to BANYAN II. They show clear signs of youth, and we adopt an 80% membership probability for the pair.

HIP 99273—This mid-F star, like the Tycho stars above, sees its membership probability in β Pic drop from 99.9% to $\sim$80% from BANYAN to BANYAN II. Given the (unsurprising for its temperature) lack of secondary age indicators to confirm its youth, we adopt the latter probability.

HIP 104308—This A star is a proposed member of TW Hya (Zuckerman & Song 2004). Malo et al. (2013) find a 99% probability of membership when neglecting RV data, which consist of a single uncertain measurement by Zuckerman & Song (2004). The addition of the radial velocity, though at -10 ± 10 km s^{-1}, only 1σ away from the TW Hya distribution of -0.2 ± 3.5 km s^{-1}, reduces BANYAN's membership probability to zero (for comparison, HIP 95261 lies 5σ from its predicted radial velocity). We decline to draw such a strong conclusion, adopting an 80% membership probability.

TABLE 1
SECONDARY AGE INDICATORS

Name HIP/HD/GJ/Other	Moving Group	Prob. Member[a]	$\log R'_{\rm HK}$[b]	$\log R_{\rm X}$[c]	Li EW (mÅ)/ $\log$ A[d]	$P_{\rm rot}$ (days)	References[e]
SEEDS Debris Disk Targets							
HIP 682	...	...	−4.38	−4.15	150	...	T06
HIP 5944	...	...	−4.47	−4.68	[A] 2.73	5.67	Mi12, G00
HIP 6878	...	...	−4.43	−4.34	48	3.13	W07, W11
HIP 7345	...	...	...	<−5.89	...	...	...
HIP 7576	β Pic	95+	−4.49	−4.43	103	7.15	L06, S09
HIP 9141	Tuc-Hor	95+	−4.22	−3.97	190	3.02	T06, W11
HIP 11360	Columba	85	...	−4.86	...	...	...
HIP 11847	β Pic	50	...	<−4.69	...	...	...
HIP 13402	β Pic	20	−4.36[MW]	−3.90	224	6.76	W07, W11
HIP 18859	AB Dor	95+	−4.40	−4.16	...	...	...
HD 281691	...	...	−3.97	−3.13[B]	345	2.65	W07, W11
HIP 22845	...	...	...	<−6.31	...	...	...
HIP 28103	...	...	...	−5.75	...	...	...
HIP 37170	...	...	−4.38	−4.26	107	...	W07
HIP 40693	...	...	−5.03	−5.90	2.5	...	T05
HD 70573	...	...	−4.16	−4.09	166	3.30	W07, S09
HIP 42333	...	...	−4.55	−4.78[B]	[A] 2.35	6.14	T05, G00
HIP 42430	...	...	−5.11	−6.03[B]	...	...	...
HIP 42438	UMa	60	−4.37[MW]	−4.45	120	4.89	W07, G00
HIP 43726	...	...	−4.64[MW]	−5.25	19	...	T05
HIP 49809	...	...	...	−6.22	...	...	...
HIP 51658	...	...	...	<−6.27	...	...	...
HIP 52462	...	...	−4.40	−4.37	138	13.5	T06, S09
HIP 57632	Argus	90	...	<−7.29	...	...	...
HIP 58876	...	...	−4.36	−4.36	122	...	W07
HIP 59774	UMa	95+	...	<−6.77	...	...	...
HIP 60074	...	...	−4.33	−4.33	123	7.13	W07, K02
HIP 61174	...	...	...	−5.59	...	...	...
HIP 61498	TW Hya	95+	...	−5.24	550[s]	...	D09
HIP 61960	...	...	...	<−6.22	...	...	...
HIP 63076	...	...	...	<−6.08	...	...	...
HIP 63584	...	...	...	−5.00[B]	...	...	...
HIP 69732	...	...	...	<−6.80	...	...	...
HIP 70952	...	...	...	−5.03	...	...	...
HIP 71284	...	...	...	−5.55	3	...	T05
HIP 71395	...	...	−4.52	−4.47	[A] −0.3	11.5	M08, W11
HIP 74702	...	...	−4.50	<−5.18	1.4	5.97	G09, G00

TABLE 1
Secondary Age Indicators

HIP 76267	UMa	95+	...	−6.64	...	...	...
HIP 76829	β Pic	84	...	−4.98	...	...	...
HIP 77542	...[PMS]	...	...	−4.45[B]	500[s]	...	F08
HIP 79977	USco	95+	...	<−4.27	66	...	C11
HIP 82587	...	...	...	−5.54	...	...	...
HIP 87108	...	...	...	<−6.61	...	...	...
HIP 87558	...	...	...	−5.33	...	...	...
HIP 92919	...	...	−4.23	−3.12	20	2.91	W07, P05
HIP 95793	...	...	...	<−5.80	...	...	...
HIP 99711	...	...	−4.64	−5.07	[A] −0.24	24.0	G10, S09
HIP 107649	...	...	−4.87	−5.61	38	...	T06
non-SEEDS GDPS Targets							
HIP 919	...	...	−4.35	−4.19	122	6.05	W07, W11
HD 1405	AB Dor	95+	...	−2.90	267	1.76	D09, M10
HIP 4907	...	...	−4.48	−4.73	...	12.2	S09
HIP 7235	...	...	−4.63	−5.14	...	...	...
HIP 9291	Columba	75	...	−3.04	...	...	...
HIP 11072	...	...	−5.00	−4.51	50	...	T06
HIP 12530	...	...	−4.45	−4.54	...	...	...
HIP 12926	...	...	−4.93	<−5.08	...	...	...
HIP 13081	...	...	−4.57	−4.47	...	...	...
HIP 14150	...	...	−4.86	−6.03	3	...	T05
HIP 14954	...	...	−4.55	<−6.10	12	...	T05
HIP 15323	...	...	−4.47	−4.49	[A] 2.67	...	Go10
BD−19 660	...	...	...	<−3.53	...	...	...
HIP 16537	...	...	−4.52[MW]	−4.68	1	11.68	T05, W11
HIP 17695	...	...	...	−3.07	0	3.87	D09, M10
HIP 21482	...	...	−4.06	−3.05	[A] 0.47	...	Mi12
HIP 22449	...	...	−4.71	−4.99	...	...	...
HIP 23200	β Pic	95+	−4.06	−3.20	270	1.86	T06, W11
HIP 30920	...	...	...	−3.30[B]	...	0.39	W11
HIP 37766	...	...	−3.62	−3.00	...	2.78	W11
HIP 43410	...	...	−4.50[MW]	−4.35	...	...	...
HIP 44458	...	...	−4.30	−3.93[B]	170	2.86	W07, W11
HD 78141	...	...	...	−3.86	...	...	...
HIP 46816	...	...	−4.02	−3.01	245	1.70	W07, W11
HIP 51386	...	...	−4.46	−4.19	130	2.60	W07, W11
HIP 51931	...	...	−4.55	−4.92	...	...	...
HIP 52787	...	...	−4.46	−4.42	100	...	T06
HIP 54745	...	...	−4.42	−4.52	[A] 2.55	7.60	M08, W11
HIP 57370	...	...	−4.59	−5.12	[A] 0.46	12.3	G10, W11
HIP 57494	...	...	−4.92	<−4.35	...	...	...
HD 108767B	...	...	...	−4.47	...	...	...
BD+60 1417	...	...	...	−4.20	...	...	...
HIP 62523	...	...	−4.62	−5.08	[A] 1.5	15.8	M08, S09
HIP 63742	AB Dor	95+	−4.43	−4.26	142	6.47	D09, W11
HIP 65016	...	...	−4.91	<−4.47	...	...	...
HIP 65515	...	...	−4.47	−4.36	[A] 1.65	4.27	M08, S09
HIP 67092	...	...	...	<−4.11	...	...	...
HIP 69357	...	...	−4.60	−5.27	...	...	...
HD 234121	...	...	−4.28	−4.61	...	...	...
HIP 71631	...	...	−4.19[MW]	−3.52	196	2.67	W07, W11
HIP 72146	...	...	−4.93	<−5.08	...	...	...
HIP 72339	...	...	−4.72	<−4.93	[A] 0.38	...	G10
HIP 72567	...	...	−4.46	−4.65	[A] 2.8	7.85	M08, S09
HIP 74045	...	...	−3.99	−2.92[B]	228	1.90	W07, W11
HIP 75829	...	...	−4.40	−3.80	145	...	W07
HIP 77408	...	...	−4.46	−4.41	[A] 0.50	14.05	M08, W11
HIP 79755	...	...	−4.92	−4.39	...	...	...
HIP 80824	...	...	−5.31	−5.11	...	...	...
HIP 81084	...	...	−4.53	−3.45	0	7.45	D09, M10
HIP 86346	AB Dor	95+	...	−3.02	40	1.84	D09, M10
HIP 87322	...	...	...	<−4.40	...	...	...
HIP 88848	...	...	−4.14	−2.98	179	...	W07
HIP 89005	...	...	...	−3.95	11	...	G09
HIP 97438	...	...	−3.77	−4.69	87	...	G09
HIP 101262	...	...	...	−4.99	...	...	...
HIP 104225	...	...	−4.97	<−5.24	...	...	...
HIP 105038	...	...	−4.56	−5.09	[A] −0.75	...	M08
HIP 106231	AB Dor	95+	...	−3.09	215	0.42	D09, M10
HIP 108156	...	...	−4.90	−5.23	[A] 0	4.51	M08, S09
V383 Lac	...	...	...	−3.06	270	2.47	W07, W11
HIP 112909	...	...	...	−3.06	...	1.64	N07
HIP 113020	...	...	...	<−4.16	...	...	...
HIP 115147	Columba	80	−4.16	−3.15	[A] 2.3	...	M08

TABLE 1
Secondary Age Indicators

HIP 116215	β Pic	20	−4.47	−4.51	0	...	T06
HIP 116384	...	...	...	−3.60	15	...	T06
HIP 117410	...	...	...	−3.47	0	...	T06
non-SEEDS, non-GDPS NICI Moving Group ADI Targets							
HIP 560	β Pic	95+	...	−5.27	87	...	T06
HIP 1481	Tuc-Hor	95+	−4.37	−4.12	130	...	D09
HIP 2729	Tuc-Hor	95+	...	−3.23	360	0.37	D09, M10
HIP 5191	AB Dor	95+	...	−3.68	155	7.13	D09, M10
HIP 9685	Tuc-Hor	95+	...	−4.92	60	...	T06
HIP 12394	Tuc-Hor	95+	...	<−6.42	0	...	D09
TYC 8491-656-1	Tuc-Hor	95+	...	−2.99	298	1.28	D09, M10
AF Hor	Tuc-Hor	95+	...	−2.59	10	0.56	D09, K12
TYC 8497-995-1	Tuc-Hor	95+	...	−3.55	120	7.4	D09, M10
HIP 14684	AB Dor	95+	−4.38	<−4.27	191	5.5	D09, M10
TYC 5899-26-1	AB Dor	95+	...	−3.10	20	...	D09
TYC 8513-952-3	AB Dor	95+	...	−2.92	0	1.5	D09, M10
HIP 23309	β Pic	95+	...	−3.42	294	8.6	F08, M10
HIP 25283	AB Dor	95+	−4.32	−3.64	15	9.3	D09, M10
HIP 26373	AB Dor	95+	−4.21	−3.17	285	4.5	D09, M10
TYC 5361-1476-1	AB Dor	90	...	−3.50	230	5.6	D09, K12
TYC 7084-794-1	AB Dor	95+	...	−3.12	10	1.7	D09, M10
HIP 29964	β Pic	95+	−4.16	−2.83	357	2.7	F08, M10
HIP 30034	Car	95+	...	−3.16	320	3.9	D09, M10
HIP 30314	AB Dor	95+	−4.34	−4.14	150	0.48	D09, R12
GSC 08894-00426	AB Dor	95+	...	−2.84	0	1.0	D09, K12
GJ 9251 A	AB Dor	...	...	<−4.07	...	...	...
TWA 6	TW Hya	95+	...	−2.88	560	0.54	F08, M10
TWA 7	TW Hya	95+	...	−3.19	530	5.0	T06, M10
HIP 53911	TW Hya	95+	...	−2.12	426	2.8	F08, M10
TWA 14	TW Hya	95+	...	−2.89	600	0.63	F08, M10
TWA 13N	TW Hya	95+	...	−2.82	570	5.6	F08, M10
TWA 8A	TW Hya	95+	...	−2.92	530	4.7	F08, M10
TWA 9B	TW Hya	95+	...	−2.30	480	4.0	D09, M10
HIP 57589	TW Hya	95+	...	−2.88	470	5.0	F08, M10
TWA 25	TW Hya	95+	...	−3.05	494	5.1	F08, M10
TWA 20	TW Hya	95+	...	−3.37	160	0.65	F08, M11
TWA 10	TW Hya	95+	...	−3.02	460	8.4	F08, M10
TWA 11B	TW Hya	95+	...	−3.12	550	...	D09
TWA 11A	TW Hya	95+	...	−5.27	550	...	D09
HD 139084B	β Pic	95+	...	-1.58^{B}	260	4.3	F08, M10
HD 155555C	β Pic	95+	...	-1.67^{B}	250	1.7	D09, M10
TYC 8728-2262-1	β Pic	50	...	−3.08	360	1.8	D09, M10
HD 164249B	β Pic	95+	...	-3.01^{B}	92	...	F08
HIP 92024	β Pic	95+	...	−5.64	490	0.35	T06, M10
TYC 9073-762-1	β Pic	80	...	−3.21	332	5.4	D09, M10
TYC 7408-54-1	β Pic	80	...	−3.04	492	1.1	D09, M10
HIP 92680	β Pic	95+	−3.82	−3.13	287	1.0	D09, M10
HIP 95261	β Pic	50	...	<−5.73	...	...	...
HIP 95270	β Pic	95+	...	<−4.39	120	...	D09
2MASS J19560294-3207186	β Pic	80	...	-2.85^{B}	500	...	Mc12
TYC 7443-1102-1	β Pic	80	...	-3.00^{B}	110	12	M11, Mc12
HIP 99273	β Pic	80	−4.59	−4.83	58	...	W07
HIP 104308	Tuc-Hor	80	...	<−5.34	...	...	...
HIP 107345	Tuc-Hor	95+	...	−3.22	55	4.5	D09, M10
TYC 9340-437-1	β Pic	95+	...	−2.90	440	4.5	D09, M10
HIP 112312	β Pic	95+	...	-2.68^{B}	0	2.4	D09, M10
TX PsA	β Pic	95+	...	-2.31^{B}	450	...	D09
TYC 5832-666-1	β Pic	95+	...	−3.05	185	5.7	D09, M10
HIP 118121	Tuc-Hor	95+	...	−5.79	...	...	...
Additional HiCIAO Detections							
HIP 64792 (GJ 504)	...	...	-4.45^{MW}	−4.42	83	3.3	T05, M03
HIP 95319 (GJ 758)	...	...	−5.08	<−5.04	2	...	T05

TABLE 1
Secondary Age Indicators

[a] High-probability (95%+) members typically have a 99%+ membership probability from Banyan (Malo et al. 2013), or a 95%+ probability from Banyan ii (Gagné et al. 2014), plus an additional youth indicator. See Section 3.4 for details on other stars.
[b] From the catalog compiled by Pace (2013); see text for details. All targets bluer than $B - V = 0.45$ have been omitted.
[c] From the *ROSAT* satellite; see text for details.
[d] Logarithmic lithium abundances, A(H) = 12, are preceded by [A]. The other values are equivalent widths.
[e] References abbreviated as: C11 (Chen et al. 2011); D09 (da Silva et al. 2009); F08 (Fernández et al. 2008); G00 (Gaidos et al. 2000); G09 (Guillout et al. 2009); G10 (Ghezzi et al. 2010); K02 (Koen & Eyer 2002); K12 (Kiraga 2012); L06 (López-Santiago et al. 2006); M96 (Messina & Guinan 1996); M03 (Messina et al. 2003); M08 (Mishenina et al. 2008); M10 (Messina et al. 2010); M11 (Messina et al. 2011); Mi12 (Mishenina et al. 2012); Mc12 (McCarthy & White 2012); N07 (Norton et al. 2007); P05 (Pojmanski et al. 2005); S09 (Samus et al. 2009); T06 (Torres et al. 2006), T05 (Takeda & Kawanomoto 2005); W07 (White et al. 2007); W11 (Wright et al. 2011)
[s] Equivalent width in the secondary
[B] The star has a known binary companion that could contribute X-ray flux.
[MW] $R'_{\rm HK}$ from multi-decade Mt. Wilson measurements (Baliunas et al. 1995; Radick et al. 1998; Lockwood et al. 2007)
[PMS] Pre-main-sequence object with an age of 5 ± 1 Myr

4. BAYESIAN AGES

We revisit the age estimates of all targets in our sample using the method detailed in Brandt et al. (2014), which we summarize here. Our method combines a possible identification with a MG of known age with secondary age indicators, including chromospheric and X-ray activity and stellar rotation. We use the MGs identified in that paper, to which we refer for discussion and references:

1. β Pictoris (21 ± 4 Myr)
2. AB Doradus (130 ± 20 Myr)
3. Columba (30^{+20}_{-10} Myr)
4. Tucana-Horologium (30^{+10}_{-20} Myr)
5. TW Hydrae (10 ± 5 Myr)
6. Ursa Major (500 ± 100 Myr)

We treat all age uncertainties as 2σ limits, and approximate the age probability distribution for each group as a Gaussian. Our sample also contains one star each from Upper Scorpius, Argus, and Carina. Upper Scorpius is a nearby very young (∼10 Myr) starforming region (de Zeeuw et al. 1999), while Argus and Carina have similar ages to Columba (∼30 Myr, Torres et al. 2008).

We estimate the membership probability $p_{\rm MG}$ for each star as described in Section 3.4, basing our own probabilities primarily on the Banyan and Banyan ii Bayesian analyses, and capping the membership probability at 95%. The probability distribution $\mathcal{P}(\tau)$ for the stellar age is then

$$\mathcal{P}(\tau) = p_{\rm MG}\mathcal{P}_{\rm MG}(\tau) + (1 - p_{\rm MG})\,\mathcal{P}(\tau|{\rm indic}) \ , \qquad (2)$$

where $\mathcal{P}_{\rm MG}$ is the probability distribution for the age of the MG and $\mathcal{P}(\tau|{\rm indic})$ is the probability distribution for the age given the observed activity and rotation indicators. We calculate this probability distribution as described in Brandt et al. (2014); we summarize the method here.

Main-sequence stars cooler than spectral type late-F have large convective zones in their outer regions. These regions support magnetic dynamos powered by the stellar differential rotation, which drive chromospheric and coronal activity and magnetized stellar winds. Over time, the stellar wind carries away angular momentum, and the star spins down. Stellar rotation, X-ray, and chromospheric activity in the Ca ii HK line all therefore decline with time, and may be calibrated as crude clocks. These calibrations depend on the properties of the convective zone, generally parametrized using $B - V$ color for main-sequence stars. Young stars also spend a variable amount of time (longer for cooler stars) on a rapidly rotating C-sequence before approaching solid-body rotation and beginning to spin down.

Mamajek & Hillenbrand (2008) have calibrated each of these secondary indicators, $R_{\rm X}$ (the ratio of X-ray to bolometric power), $R'_{\rm HK}$ (the ratio of energy in Ca ii HK emission to the underlying photospheric continuum), and rotation period, using a large sample of Solar-type stars. We use each of these calibrations, with a correction for the time a star takes to settle on the slowly rotating I-sequence, as described in Brandt et al. (2014) and references therein. We do not assume the chromospheric and coronal activity measurements to be independent age indicators, but rather treat them both as proxies for the Rossby number (the ratio of the rotation period to the convective overturn timescale τ_C), which we convert to an age using a color-dependent estimate of τ_C and the period-age relations.

We then combine the activity age distribution with that inferred directly from the rotation period (if measured) and add an additional 15% (0.06 dex) to account for systematic uncertainties. We also add a 5% probability that the star is a pathological case, in the sense that its secondary age indicators do not correspond to its actual age and are useless for dating. Multiplying the resulting distribution by a prior uniform in time out to either 10 Gyr or the star's color-dependent main sequence lifespan gives $\mathcal{P}(\tau|{\rm indic})$. Finally, we weight $\mathcal{P}(\tau|{\rm indic})$ by $1-p_{\rm MG}$, the probability that the star is *not* a member of a well-defined MG, and use it in Equation (2).

When drawing ages for each star from these probability distributions, we account for the fact that the ages of each member of a MG should be the same. We first draw the ages for each of the MGs, then assign each suggested group member either to its group or to the field, and finally draw an age for each field star from its posterior age probability distribution. Given the large number of stars, the central limit theorem drives the predicted number of

substellar companions to a relatively narrow Gaussian given a fixed substellar distribution function.

Table 2 lists the ages (in Myr) at 5%, 10%, 25%, 50%, 75%, 90%, and 95% of the cumulative posterior probability. The range of ages between the 25% and 75% levels thus contains half of the posterior probability, while the range from 5% to 95% contains nine-tenths of the posterior probability, and may be used as a 90% confidence age interval. We use the full posterior probability distributions summarized in Table 2 throughout the rest of our analysis. A few of these differ significantly from the distributions in Brandt et al. (2014); these targets had their Ca II HK and/or X-ray activity incorrectly input into the earlier paper's calculation.

TABLE 2
Age Distributions of All Targets

Name HIP/HD/GJ/Other	RA (J2000) (h m s)	Dec (J2000) (° ′ ″)	Age at Posterior CDF Value (Myr) 5%	10%	25%	50%	75%	90%	95%
HIP 544	00 06 36.8	+29 01 17	192	208	237	272	311	356	421
HIP 560	00 06 50.1	−23 06 27	17	18	19	21	22	24	27
HIP 682	00 08 25.7	+06 37 00	21	43	108	217	343	498	725
HIP 919	00 11 22.4	+30 26 58	205	221	251	287	326	372	436
HIP 1134	00 14 10.3	−07 11 57	21	23	26	30	37	45	56
HD 1405	00 18 20.9	+30 57 22	109	115	122	129	136	142	146
HIP 1481	00 18 26.1	−63 28 39	13	17	23	30	33	37	41
FK Psc	00 23 34.7	+20 14 29	19	20	194	300	389	455	510
HIP 2729	00 34 51.2	−61 54 58	13	17	23	30	33	37	40
HIP 3589	00 45 50.9	+54 58 40	111	115	122	129	137	143	148
HIP 4907	01 02 57.2	+69 13 37	686	732	812	912	1030	1160	1320
HIP 4979	01 03 49.0	+01 22 01	152	304	766	1530	2300	2760	2920
HIP 5191	01 06 26.2	−14 17 47	113	117	123	130	138	146	168
HIP 5944	01 16 29.3	+42 56 22	323	346	388	440	500	572	668
HIP 6869	01 28 24.4	+17 04 45	787	876	1040	1240	1510	1880	2500
HIP 6878	01 28 34.4	+42 16 04	226	255	304	367	458	660	2870
HIP 7235	01 33 15.8	−24 10 41	1340	1500	1810	2200	2680	3240	3740
HIP 7345	01 34 37.8	−15 40 35	62	124	313	625	938	1130	1200
HS Psc	01 37 23.2	+26 57 12	111	116	122	130	137	144	149
HIP 7576	01 37 35.5	−06 45 38	17	18	19	21	22	24	29
HIP 9141	01 57 49.0	−21 54 05	13	17	23	30	34	38	50
HIP 9291	01 59 23.5	+58 31 16	21	23	27	33	47	304	561
HIP 9685	02 04 35.1	−54 52 54	13	17	23	30	34	38	46
HIP 10679	02 17 24.7	+28 44 30	17	18	19	21	22	24	26
HIP 11072	02 22 32.5	−23 48 59	1820	2000	2340	2770	3280	3860	4330
HIP 11360	02 26 16.2	+06 17 33	22	24	27	32	41	1610	3220
BD+30 397B	02 27 28.0	+30 58 41	17	18	19	21	22	24	26
HIP 11437	02 27 29.3	+30 58 25	17	18	19	21	22	24	29
HIP 11847	02 32 55.8	+37 20 01	18	19	20	25	2120	3400	3820
HIP 12394	02 39 35.4	−68 16 01	13	17	23	30	33	37	43
HIP 12530	02 41 14.0	−00 41 44	188	267	421	1310	3730	5180	5670
HIP 12545	02 41 25.9	+05 59 18	17	18	19	21	22	24	25
TYC 8491-656-1	02 41 46.8	−52 59 52	13	17	23	30	33	37	40
AF Hor	02 41 47.3	−52 59 31	13	17	23	30	33	37	41
HIP 12638	02 42 21.3	+38 37 07	113	117	123	130	138	146	169
TYC 8497-995-1	02 42 33.0	−57 39 37	13	17	23	30	34	38	51
HIP 12925	02 46 14.6	+05 35 33	13	17	23	30	33	37	42
HIP 12926	02 46 15.2	+25 39 00	4260	4760	5560	6570	7770	8950	9470
HIP 13081	02 48 09.1	+27 04 07	810	937	1170	1480	1860	2320	2780
HIP 13402	02 52 32.1	−12 46 11	19	20	218	284	333	380	425
HIP 14150	03 02 26.0	+26 36 33	2920	3230	3760	4420	5200	6040	6670
HIP 14684	03 09 42.3	−09 34 47	113	117	123	130	138	146	161
HIP 14954	03 12 46.4	−01 11 46	371	433	550	708	905	1160	1440
HIP 15323	03 17 40.0	+31 07 37	179	233	314	416	544	708	928
BD−19 660	03 20 50.7	−19 16 09	820	1310	2770	5180	7590	9040	9510
HIP 16537	03 32 55.8	−09 27 30	619	659	728	812	909	1020	1160
HIP 17248	03 41 37.3	+55 13 07	21	23	26	30	37	45	54
HD 23061	03 42 55.1	+24 29 35	116	118	121	124	128	131	133
TYC 1803-1406-1	03 43 27.1	+25 23 15	116	118	121	124	128	131	133
HD 23247	03 44 23.5	+24 07 58	116	118	121	124	128	131	133
BD+23 514	03 45 41.9	+24 25 53	116	118	121	124	128	131	133
V1171 Tau	03 46 28.4	+24 26 02	116	118	121	124	128	131	133
HD 23514	03 46 38.4	+22 55 11	116	118	121	124	128	131	133
HD 282954	03 46 38.8	+24 57 35	116	118	121	124	128	131	133
H II 1348	03 47 18.1	+24 23 27	116	118	121	124	128	131	133
HIP 17695	03 47 23.3	−01 58 20	67	84	132	211	291	339	365
HD 23863	03 49 12.2	+23 53 12	116	118	121	124	128	131	133
H II 2311	03 49 28.7	+23 42 44	116	118	121	124	128	131	133
HD 23912	03 49 32.7	+23 22 49	116	118	121	124	128	131	133
H II 2366	03 49 36.5	+24 17 46	116	118	121	124	128	131	133
H II 2462	03 49 50.4	+23 42 20	116	118	121	124	128	131	133
BD+22 574	03 49 56.5	+23 13 07	116	118	121	124	128	131	133
V1174 Tau	03 50 34.6	+24 30 28	116	118	121	124	128	131	133
HIP 18050	03 51 27.2	+24 31 07	116	118	121	124	128	131	133
V1054 Tau	03 51 39.3	+24 32 56	116	118	121	124	128	131	133

TABLE 2
Age Distributions of All Targets

V885 Tau	03 53 45.3	+25 55 34	116	118	121	124	128	131	133
HIP 18859	04 02 36.7	−00 16 08	112	116	123	130	137	144	150
HD 281691	04 09 09.7	+29 01 30	52	61	80	107	134	159	225
HIP 21482	04 36 48.2	+27 07 56	22	46	116	234	358	477	662
HIP 22449	04 49 50.4	+06 57 41	315	630	1400	2770	4340	5280	5600
TYC 5899-26-1	04 52 24.4	−16 49 22	112	116	123	130	137	145	152
TYC 8513-952-3	04 53 31.2	−55 51 37	110	115	122	129	136	143	148
HIP 22845	04 54 53.7	+10 09 03	67	136	339	679	1020	1220	1300
HIP 23200	04 59 34.8	+01 47 01	17	18	19	21	22	24	26
HIP 23309	05 00 47.1	−57 15 25	17	18	19	21	22	24	29
HIP 23362	05 01 25.6	−20 03 07	21	23	26	30	37	45	55
HIP 25283	05 24 30.2	−38 58 11	113	117	123	130	138	146	169
HIP 25486	05 27 04.8	−11 54 03	17	18	19	21	22	24	25
HD 36869	05 34 09.2	−15 17 03	21	23	26	30	37	45	51
HIP 26373	05 36 56.9	−47 57 53	113	117	123	130	137	145	152
HIP 28103	05 56 24.3	−14 10 04	197	400	1000	2010	3010	3610	3820
TYC 5361-1476-1	06 02 21.9	−13 55 33	113	117	124	131	139	152	232
HIP 29067	06 07 55.3	+67 58 37	96	193	439	673	941	1280	1690
TYC 7084-794-1	06 09 19.2	−35 49 31	110	115	122	129	137	143	148
HIP 29964	06 18 28.2	−72 02 41	17	18	19	21	22	24	28
HIP 30030	06 19 08.1	−03 26 20	21	23	26	30	37	45	51
HIP 30034	06 19 12.9	−58 03 16	30	32	36	40	44	49	62
HIP 30314	06 22 30.9	−60 13 07	102	114	122	129	136	142	146
GSC 08894-00426	06 25 56.1	−60 03 27	110	115	122	129	136	143	147
HIP 30920	06 29 23.4	−02 48 50	8	18	50	112	195	277	339
HIP 32104	06 42 24.3	+17 38 43	21	23	26	30	37	46	58
V429 Gem	07 23 43.6	+20 24 59	111	116	122	130	137	143	148
HIP 37170	07 38 16.4	+47 44 55	24	50	127	255	393	562	806
HIP 37288	07 39 23.0	+02 11 01	1580	1780	2150	2620	3180	3830	4390
HIP 37766	07 44 40.2	+03 33 09	45	61	106	181	256	300	331
GJ 9251A	08 07 09.1	+07 23 00	840	1340	2800	5190	7600	9030	9520
FP Cnc	08 08 56.4	+32 49 11	23	25	29	50	169	243	267
HIP 40693	08 18 23.9	−12 37 56	4360	4840	5630	6620	7840	9020	9510
HIP 40774	08 19 19.1	+01 20 20	181	355	584	840	1160	1570	2030
HD 70573	08 22 50.0	+01 51 34	107	118	140	168	197	226	266
HIP 42333	08 37 50.3	−06 48 25	332	355	399	451	512	585	684
HIP 42430	08 39 07.9	−22 39 43	4520	5020	5850	6900	8190	9260	9640
HIP 42438	08 39 11.7	+65 01 15	238	261	315	457	514	554	580
HIP 43410	08 50 32.2	+33 17 06	267	299	359	437	532	654	833
HIP 43726	08 54 17.9	−05 26 04	1220	1340	1560	1840	2170	2570	2960
HIP 44458	09 03 27.1	+37 50 28	100	111	132	160	188	215	250
HIP 44526	09 04 20.7	−15 54 51	282	305	346	395	448	508	589
HD 78141	09 07 18.1	+22 52 22	26	54	139	279	448	810	1370
HIP 45383	09 14 53.7	+04 26 34	41	83	207	409	620	872	1210
HIP 46816	09 32 25.6	−11 11 05	25	32	52	84	117	137	148
HIP 46843	09 32 43.8	+26 59 19	164	178	204	236	270	308	362
HIP 49809	10 10 05.9	−12 48 57	207	418	1050	2100	3150	3780	4000
HIP 50156	10 14 19.2	+21 04 30	22	24	27	33	45	341	405
TWA 6	10 18 28.7	−31 50 03	5	6	8	10	11	13	16
GJ 388	10 19 36.3	+19 52 12	41	56	104	182	261	308	327
HIP 50660	10 20 45.9	+32 23 54	1170	1350	1680	2110	2640	3260	3830
HIP 51317	10 28 55.6	+00 50 28	113	117	123	130	138	146	169
HIP 51386	10 29 42.2	+01 29 28	100	112	135	164	195	228	277
HIP 51658	10 33 13.9	+40 25 32	126	253	636	1270	1910	2290	2430
HIP 51931	10 36 30.8	−13 50 36	948	1090	1340	1680	2090	2580	3060
TWA 7	10 42 30.1	−33 40 17	5	6	8	10	12	14	21
HIP 52462	10 43 28.3	−29 03 51	612	653	725	813	915	1040	1180
HIP 52787	10 47 31.2	−22 20 53	285	441	619	840	1120	1460	1860
HIP 53020	10 50 52.0	+06 48 29	4600	5160	6140	7500	8820	9550	9780
HIP 53486	10 56 30.8	+07 23 19	501	535	595	669	755	856	984
HD 95174	10 59 38.3	+25 26 15	20	23	358	3790	6890	8760	9380
HIP 53911	11 01 51.9	−34 42 17	5	6	8	10	12	14	20
HIP 54155	11 04 41.5	−04 13 16	24	49	125	251	392	576	870
HIP 54745	11 12 32.4	+35 48 51	412	440	491	553	624	709	820
TWA 14	11 13 26.2	−45 23 43	5	6	8	10	11	13	16
TYC 3825-716-1	11 20 50.5	+54 10 09	28	57	145	292	471	777	1320
TWA 13N	11 21 17.2	−34 46 46	5	6	8	10	12	14	21
TWA 8A	11 32 41.3	−26 51 56	5	6	8	10	12	14	21
HIP 57370	11 45 42.3	+02 49 17	741	790	876	983	1110	1260	1430
HIP 57494	11 47 03.8	−11 49 27	3870	4310	5040	5940	7040	8290	9050
TWA 9B	11 48 23.7	−37 28 49	5	6	8	10	12	14	21
HIP 57589	11 48 24.2	−37 28 49	5	6	8	10	12	14	21
HIP 57632	11 49 03.6	+14 34 19	30	33	37	42	50	1090	1510
HIP 58876	12 04 33.7	+66 20 12	19	39	97	194	304	437	635
G 123-7	12 09 37.3	+40 15 07	1530	1720	2060	2500	3020	3640	4170
TYC 4943-192-1	12 15 18.4	−02 37 28	109	115	123	131	141	304	484
HIP 59774	12 15 25.6	+57 01 57	411	433	465	501	537	572	601

TABLE 2
Age Distributions of All Targets

TWA 25	12 15 30.7	−39 48 43	5	6	8	10	12	14	21
HIP 60074	12 19 06.5	+16 32 54	349	373	417	470	532	606	704
HIP 60661	12 25 58.6	+08 03 44	2880	3210	3780	4500	5330	6240	6900
HD 108767B	12 29 50.9	−16 31 15	77	158	401	761	1240	1860	2520
TWA 20	12 31 38.1	−45 58 59	5	6	8	10	11	13	16
HIP 61174	12 32 04.2	−16 11 46	220	441	1100	2200	3310	3970	4190
TWA 10	12 35 04.3	−41 36 39	5	6	8	10	12	14	21
TWA 11B	12 36 00.6	−39 52 16	5	6	8	10	12	14	17
HIP 61498	12 36 01.0	−39 52 10	5	6	8	10	12	14	17
TWA 11A	12 36 01.0	−39 52 10	5	6	8	10	12	14	17
HIP 61960	12 41 53.1	+10 14 08	64	129	323	647	969	1160	1240
BD+60 1417	12 43 33.3	+60 00 53	35	72	184	376	694	1180	1780
HIP 62523	12 48 47.0	+24 50 25	1210	1290	1430	1590	1780	2000	2230
HIP 63076	12 55 28.5	+65 26 19	173	347	871	1740	2610	3140	3320
HIP 63317	12 58 32.0	+38 16 44	20	42	107	216	330	442	638
HIP 63584	13 01 46.9	+63 36 37	253	510	1280	2560	3850	4620	4880
HIP 63742	13 03 49.7	−05 09 43	113	117	123	130	138	146	164
HIP 64792	13 16 46.5	+09 25 27	166	180	205	236	268	303	352
HIP 65016	13 19 40.1	+33 20 48	3680	4080	4770	5620	6630	7810	8650
HIP 65515	13 25 45.5	+56 58 14	110	121	142	171	199	227	266
FH CVn	13 27 12.1	+45 58 26	41	60	111	130	154	209	228
HIP 66252	13 34 43.2	−08 20 31	75	88	120	173	226	259	287
HIP 67092	13 45 05.3	−04 37 13	880	1380	2820	5210	7600	9040	9520
HIP 67412	13 48 58.2	−01 35 35	1280	1440	1740	2130	2600	3150	3660
HIP 69357	14 11 46.2	−12 36 42	1390	1570	1890	2310	2810	3400	3920
HD 234121	14 16 12.2	+51 22 35	16	34	87	177	279	413	623
HIP 69732	14 16 23.0	+46 05 18	67	136	343	689	1030	1240	1320
HIP 70952	14 30 46.1	+63 11 09	258	518	1300	2590	3890	4670	4930
HIP 71284	14 34 40.8	+29 44 42	211	427	1070	2140	3210	3850	4070
HIP 71395	14 36 00.6	+09 44 47	501	536	598	673	760	862	992
HIP 71631	14 39 00.2	+64 17 30	76	85	104	131	157	180	209
HIP 72146	14 45 24.2	+13 50 47	4270	4760	5580	6580	7770	8940	9470
HIP 72339	14 47 32.7	−00 16 53	2060	2320	2790	3380	4090	4880	5500
HIP 72567	14 50 15.8	+23 54 43	481	514	572	643	726	824	945
HIP 73996	15 07 18.1	+24 52 09	296	461	884	2360	3840	4720	5020
HIP 74045	15 07 56.3	+76 12 03	29	36	59	95	132	154	166
HIP 74702	15 15 59.2	+00 47 47	187	203	232	269	309	359	434
HIP 75829	15 29 23.6	+80 27 01	33	67	173	354	554	799	1130
HIP 76267	15 34 41.3	+26 42 53	407	430	464	500	535	569	593
HD 139084B	15 38 56.8	−57 42 19	17	18	19	21	22	24	29
HIP 76829	15 41 11.4	−44 39 40	35	72	182	368	564	716	789
HIP 77408	15 48 09.5	+01 34 18	769	819	908	1020	1150	1300	1470
HIP 77542	15 49 57.7	−03 55 16	4	4	4	5	5	5	5
HIP 78557	16 02 22.4	+03 39 07	11	24	62	128	210	434	3360
HIP 79762	16 16 45.3	+67 15 23	2510	2770	3230	3800	4470	5210	5780
HIP 79977	16 19 29.2	−21 24 13	6	7	8	10	11	13	16
HIP 80824	16 30 18.1	−12 39 45	3610	3980	4610	5370	6240	7190	7860
HIP 81084	16 33 41.6	−09 33 12	162	189	255	358	460	531	655
HIP 82587	16 52 58.1	+31 42 06	185	371	923	1840	2770	3320	3510
HIP 82688	16 54 08.1	−04 20 25	111	116	122	130	137	143	148
HIP 83494	17 03 53.6	+34 47 25	127	255	637	1270	1900	2280	2420
HD 155555C	17 17 31.3	−66 57 05	17	18	19	21	22	24	25
TYC 8728-2262-1	17 29 55.1	−54 15 49	18	19	20	24	82	118	130
HIP 86346	17 38 39.6	+61 14 16	111	116	122	129	137	143	148
HIP 87108	17 47 53.6	+02 42 26	53	108	274	550	825	993	1060
HIP 87322	17 50 34.0	−06 03 01	1130	1650	3070	5390	7690	9080	9540
HIP 87558	17 53 14.2	+06 06 05	268	538	1350	2710	4070	4880	5160
HIP 87579	17 53 29.9	+21 19 31	359	489	664	891	1170	1520	1920
HIP 87768	17 55 44.9	+18 30 01	29	59	151	305	484	706	1010
HD 164249B	18 03 04.1	−51 38 56	17	18	19	21	22	24	26
HIP 88848	18 08 16.0	+29 41 28	18	38	97	196	301	405	586
HIP 89005	18 09 55.5	+69 40 50	26	54	138	280	449	804	1360
HIP 91043	18 34 20.1	+18 41 24	30	36	52	78	104	120	133
HIP 92024	18 45 26.9	−64 52 17	17	18	19	21	22	24	27
TYC 9073-762-1	18 46 52.6	−62 10 36	17	18	20	21	24	253	331
TYC 7408-54-1	18 50 44.5	−31 47 47	17	18	19	21	23	88	153
HIP 92680	18 53 05.9	−50 10 50	17	18	19	21	22	23	25
HIP 92919	18 55 53.2	+23 33 24	55	63	85	121	156	179	200
HIP 93580	19 03 32.3	+01 49 08	113	117	124	132	144	1120	1680
HIP 95261	19 22 51.2	−54 25 26	18	19	20	24	451	722	815
HIP 95270	19 22 58.9	−54 32 17	17	18	19	21	22	24	27
HIP 95319	19 23 34.0	+33 13 19	5020	5660	6720	8040	9140	9690	9860
HIP 95793	19 29 01.0	+01 57 02	68	139	353	709	1070	1280	1360
HIP 97438	19 48 15.4	+59 25 22	14	29	74	152	242	355	532
2MASS J19560294-3207186	19 56 02.9	−32 07 19	17	18	19	21	23	301	511
TYC 7443-1102-1	19 56 04.4	−32 07 38	17	18	20	21	24	485	562
HIP 99273	20 09 05.2	−26 13 27	17	18	20	21	24	2760	4130

TABLE 2
Age Distributions of All Targets

HIP 99711	20 13 59.8	−00 52 01	1670	1780	1960	2190	2440	2720	2990
HIP 101262	20 31 32.1	+33 46 33	696	898	1290	1810	2480	3270	3980
BD+05 4576	20 39 54.6	+06 20 12	47	95	124	141	334	560	854
HIP 102409	20 45 09.5	−31 20 27	17	18	19	21	22	24	29
HIP 104225	21 06 56.4	+69 40 29	4460	4980	5880	7060	8470	9420	9730
HIP 104308	21 07 51.2	−54 12 59	14	18	25	31	37	1420	2130
HD 201919	21 13 05.3	−17 29 13	113	117	123	130	137	145	152
HIP 105038	21 16 32.5	+09 23 38	1050	1190	1450	1790	2200	2690	3170
HIP 106231	21 31 01.7	+23 20 07	105	114	122	129	136	142	146
HIP 107345	21 44 30.1	−60 58 39	13	17	23	30	34	38	50
HIP 107350	21 44 31.3	+14 46 19	236	254	285	324	367	417	487
HIP 107649	21 48 15.8	−47 18 13	1680	1850	2170	2560	3030	3580	4020
HIP 108156	21 54 45.0	+32 19 43	3270	3620	4220	4960	5810	6720	7350
TYC 2211-1309-1	22 00 41.6	+27 15 14	14	18	20	23	85	166	211
V383 Lac	22 20 07.0	+49 30 12	46	53	70	98	126	145	162
HIP 111449	22 34 41.6	−20 42 30	265	537	1350	2710	4060	4880	5150
TYC 9340-437-1	22 42 48.9	−71 42 21	17	18	19	21	22	24	29
HIP 112312	22 44 58.0	−33 15 02	17	18	19	21	22	24	27
TX PsA	22 45 00.1	−33 15 26	17	18	19	21	22	24	26
HIP 112909	22 51 53.5	+31 45 15	12	21	47	96	155	202	223
HIP 113020	22 53 16.7	−14 15 49	940	1440	2870	5250	7630	9050	9520
HIP 114066	23 06 04.8	+63 55 34	113	117	123	130	137	145	151
HIP 115147	23 19 26.6	+79 00 13	21	23	27	32	43	232	356
HIP 115162	23 19 39.6	+42 15 10	112	116	123	130	137	144	150
TYC 5832-666-1	23 32 30.9	−12 15 51	17	18	19	21	22	24	29
HIP 116215	23 32 49.4	−16 50 44	19	20	436	789	1080	1400	1710
HIP 116384	23 35 00.3	+01 36 19	29	59	147	289	459	756	1260
HIP 116805	23 40 24.5	+44 20 02	21	25	34	130	293	393	430
HIP 117410	23 48 25.7	−12 59 15	26	54	138	278	445	751	1260
HIP 118121	23 57 35.1	−64 17 54	13	17	23	30	34	38	44

5. SUBSTELLAR COOLING MODELS

Objects below ∼80 $M_{\rm Jup}$ never attain the central densities and temperatures necessary to stabilize themselves by hydrogen fusion; instead, they simply cool and fade below the detectability limits of even the largest telescopes. Substellar cooling models simulate the structure and atmosphere of such an object as a function of its mass, age, and initial thermodynamic state, producing grids of spectra and luminosities. Many such models have been developed recently and are widely used (e.g. Chabrier et al. 2000; Allard et al. 2001; Baraffe et al. 2003; Marley et al. 2007; Allard et al. 2011; Spiegel & Burrows 2012). These models make a range of assumptions about dust settling, cloud structure, chemical composition, and initial thermodynamic state.

The formation mechanism of planetary mass objects is still debated, and can strongly impact their brightness at young ages. Direct gravitational collapse forms objects on a dynamical timescale (Boss 2000), giving them little time to radiate away their heat of formation. In contrast, an object formed by core-accretion accretes its gas over a viscous time, and is likely to radiate away much of its initial energy in an accretion shock (Hubickyj et al. 2005; Marley et al. 2007). However, the identification of a core-accretion formation scenario with a "cold start" is far from certain; a subcritical shock, for example, could prevent efficient cooling (Bromley & Kenyon 2011), while a very massive core could provide a substantial reservoir of heat (Mordasini 2013). Observational evidence also disfavors a very cold start for many imaged planets (Marleau & Cumming 2014). Massive brown dwarfs are generally accepted to form by direct gravitational collapse, either in a disk or a molecular cloud (Bate et al. 2002).

In this work, we explore whether the entire range of long-period substellar objects is compatible with a single distribution function. We therefore seek a single model applicable over this entire range, including the more massive brown dwarfs. Such a model would imply that all of these objects form by direct gravitational collapse, and therefore, form hot. We adopt the recent BT-Settl models (Allard et al. 2011), which incorporate clouds and dust settling in the appropriate physical regimes, and are intended to be valid all the way from ∼1 M_J up to stellar masses. BT-Settl reproduces the earlier COND/DUSTY hot-start models of Baraffe et al. (2003) and Chabrier et al. (2000) in the applicable limits.

We also explore the effects of the formation model on our results restricted to the planetary mass regime, below the deuterium-burning limit of ∼13 M_J. In this case, we parametrize our ignorance using the "warm-start" models of Spiegel & Burrows (2012), henceforth SB12. These model grids include an additional parameter—initial entropy—at each age, mass, and atmospheric composition. We restrict our analysis to a fiducial model with clouds and 3 times Solar metallicity.

Under any formation scenario, the initial entropy is likely to be a function of mass. More massive objects can attain a higher entropy while still permitting hydrostatic equilibrium, resulting in hotter starts. However, they can also radiate more effectively (and for much longer) under a core-accretion scenario, producing an initially colder object. We parametrize the range of initial thermodynamic states using a single "warmth parameter," η, to fill the space between the high- and low-entropy envelopes given by SB12:

$$S_{\rm init}(M) = \eta S_{\rm init,\,max}(M) + (1-\eta) S_{\rm init,\,min}(M)\ , \quad (3)$$

with $\eta \in [0, 1]$.

Much uncertainty remains throughout the modeling process, and we make no claim that our use of the BT-Settl and SB12 models here exhausts parameter space. We adopt the BT-Settl models in an attempt to include the entire range of substellar masses in a consistent manner, while we use the SB12 models to smoothly explore the effect of the initial thermodynamic conditions. Substellar luminosities depend strongly on both mass and age, limiting (at least somewhat) the impact of systematic errors in predicted luminosity on the expected distribution of objects detected by high-contrast imaging.

6. STATISTICAL FRAMEWORK

High-contrast imaging data provide a detection limit (or a detected companion) everywhere on the field-of-view; we want to compare these data to predictions made by models of exoplanet formation and evolution. The probability of a planet existing at any individual location around a particular star is tiny. Hence, in the absence of any other information about the star, the planet's existence is a Poisson process. If we denote by λ_i the expected number of substellar companions that exist and are detectable at a given position and luminosity i, given some detection limits and model of planet properties, then the probability of such a companion existing is $\lambda_i e^{-\lambda_i}$ ($\approx \lambda_i$), while the probability of its not existing (either because there is no companion or because it is too faint) is $e^{-\lambda_i}$ ($\approx 1-\lambda_i$). Here, i runs over both position and substellar luminosity, and the λ_i are functions of the substellar companion distribution function, cooling models, and survey contrast.

The approximation of planet occurrence as an independent Poisson process at every point around every star surveyed breaks down with multiple systems or when other information, such as stellar binarity, makes some positions more dynamically favorable than others. The famous four (or more) planet system HR 8799 illustrates this empirically. Various studies have found that few stars (typically no more than 5–10%) host massive ($\gtrsim$5 $M_{\rm Jup}$), long-period exoplanets (e.g. Lafrenière et al. 2007; Vigan et al. 2012; Nielsen et al. 2013; Chauvin et al. 2014). If planet occurrence is independent at different locations, the number of single planet systems should exceed the number of four-planet systems by at least a factor of 10^3–10^4, while the number of two-planet systems should be larger than HR8799-like systems by a factor of at least 10^2–10^3. The fact that we have not found a single system with two $\sim$5–10 $M_{\rm Jup}$ companions argues powerfully against independent occurrence probabilities, even before considering theoretical arguments.

As high-contrast surveys improve in sensitivity and target hundreds of new stars, the number of known multiple systems will almost certainly rise. However, the data sets we consider here lack any detected multiple planet systems, freeing us (for now) from the statistical and theoretical problems they present. With the caveat that our statistical framework must be abandoned or at least modified if systems like HR 8799 are to be included, we therefore proceed by assuming planet occurrence to be an independent Poisson process. The likelihood function $\mathcal{L}$, the probability density of the given data set (detected companions plus sensitivity limits) given a model of planet frequency and properties, is then the product of the planet-occurrence probabilities over all elements of the fields-of-view of all stars, and over all substellar luminosities:

$$\mathcal{L} = \prod_i e^{-\lambda_i} \times \prod_{\rm obj\ } \lambda_j e^{-\lambda_j} \ . \tag{4}$$

The index i runs over all locations around all stars and over all planet luminosities, apart from those positions and luminosities at which a companion was seen. The index j only runs over the pixels and luminosities where substellar companions were discovered. The latter term is the likelihood of finding all of the detected companions at their actual positions with their observed luminosities. The exponential term in the product over j combines with the identical term in the product over i to give a product over all pixels around all stars and over all planet luminosities, *including those where companions were discovered.* The likelihood is more conveniently written logarithmically, and reduces to

$$\ln \mathcal{L} = -\sum_i \lambda_i + \sum_{\rm obj\ } \ln \lambda_j = -\langle N_{\rm obj} \rangle + \sum_{\rm obj\ } \ln \lambda_j \ , \tag{5}$$

where now i runs over all pixels around all stars and over all companion luminosities. The first term, λ_i summed over all planet positions and luminosities, is simply the expected number of detectable companions, $\langle N_{\rm obj} \rangle$, given the substellar distribution function.

The substellar distribution function, from which the λ_i and λ_j are computed, can depend arbitrarily on parameters like the host stellar type, companion mass, separation, host metallicity, etc., as we discuss in the next section. Regardless of its functional form, the distribution function may be multiplied by a constant A, which multiplies all probabilities λ_i and λ_j (and, by extension, $\langle N_{\rm obj} \rangle$) by the same factor. This normalization constant is generally not known *à priori* and must be fit by our analysis; it gives, e.g., the total number of companions per star. Such a constant enters the likelihood calculation, Equation (5), in a particularly simple way. Multiplying the distribution function, and by extension, all λ_i and λ_j, by a constant A, the likelihood function becomes

$$\ln \mathcal{L} = -A\langle N_{\rm obj} \rangle + N_{\rm obs} \ln A + \ln \lambda_j \ , \tag{6}$$

where $N_{\rm obs}$ is the number of companions actually observed. If we hold all other parameters of the distribution fixed while determining the normalization, λ_j, $\langle N_{\rm obj} \rangle$, and $N_{\rm obs}$ are all constant, and Equation (6) is a gamma distribution. The maximum likelihood value of A is, as expected, $N_{\rm obs}/\langle N_{\rm obj} \rangle$. In other words, the maximum likelihood value of A is the one that makes the predicted number of detections $\langle N_{\rm obj}$ equal to $N_{\rm obs}$, the actual number of substellar companions seen in the survey.

Setting A equal to its maximum likelihood value, the likelihood function now reads

$$\mathcal{L} = \exp\left(-N_{\rm obs}\right) \prod_{\rm obj\ } \frac{\lambda_j}{\langle N_{\rm obj} \rangle} \ . \tag{7}$$

As a result, all we need to calculate from the substellar distribution function, cooling model, and sensitivity curves are the probabilities of detecting companions at their observed positions with their observed properties, and the total number of expected detections. In the next

section, we discuss the computation of λ_j and $\langle N_{\rm obj}\rangle$ in the case of a power-law companion distribution function.

6.1. *The Exoplanet Distribution Function*

Neglecting multiplicity, the exoplanet distribution function extends over three parameters of interest: mass M, semimajor axis a, and eccentricity e. Other orbital or orientation parameters are randomly distributed, with those distributions determined by geometry (assuming the systems to be randomly oriented). The distribution function is usually assumed to be separable, i.e.,

$$p(M,a,e) = p(M)p(a)p(e)\ . \tag{8}$$

While this is unlikely to be true in reality, and may not even be a particularly good approximation, we adopt it for lack of a specific and well-motivated alternative.

When we observe a companion, the only measurements we can usually make are of its projected separation and its luminosity at various wavelengths. It is therefore the distribution of projected separation, a function of both the semimajor axis and eccentricity distributions, that is relevant to imaging surveys. The choice of eccentricity distribution turns out to be of secondary importance to this distribution. Indeed, in the special case that the semimajor axis is a power law truncated well outside the separations being probed, the eccentricity distribution drops out altogether–$p(M,a)$ is independent of $p(e)$ (see the Appendix for details).

We derive the distribution of projected separation based on an eccentricity distribution uniform in the range from 0 to 0.8 (Cumming et al. 2008); the result is nearly identical to that obtained using a Rayleigh distribution in eccentricity with $\sigma = 0.3$ (Jurić & Tremaine 2008). For completeness, we also include a distribution based on $p(e) = 2e$, the theoretical distribution expected if the phase space density of companions is a function of energy only (Ambartsumian 1937). Full details and piecewise analytic fitting functions are provided in the Appendix.

We take the exoplanet mass distribution to be a power law $p(M) \propto M^{\beta}$, and use cooling models of substellar objects to convert mass and age to a luminosity L in a given bandpass. The azimuthal variance in the detection limit is dominated by subtraction residuals from the stellar PSF and by read noise—photon noise from the companion itself is nearly always negligible. These noise distributions are typically very nearly Gaussian. With a detection threshold of N_σ (usually 5–6), the probability of detecting a companion is therefore

$$\begin{aligned} p(\text{detect}|L) &= p(L + x > N_\sigma \cdot \sigma) \\ &= \frac{1}{2} + \frac{1}{2}\text{erf}\left(\frac{(L/L_{\rm lim} - 1)N_\sigma}{\sqrt{2}}\right)\ , \end{aligned} \tag{9}$$

where x, a Gaussian random variable with variance σ^2, represents the noise, $L_{\rm lim}$ is the formal $N_\sigma\sigma$ detection threshold, and $\sigma^2 = \sigma^2(D)$ is the annular variance in the final ADI-processed image. The total differential number of sources expected at angular separation D is

$$dN(D) = p(D)\,dD \int_0^\infty \frac{dN}{dM}\frac{dM}{dL}p(\text{detect}|L)\,dL\ . \tag{10}$$

The substellar-cooling models consist of grids in age and mass, which we interpolate using piecewise power laws. We, therefore, evaluate Equation (10) for the special case of a power law dM/dL; it reduces to a function of a single parameter with variable limits of integration. We tabulate these values, enabling us to evaluate Equation (10) to a typical accuracy of much better than 0.1% with no more than a few array lookups, $\lesssim$20 floating point operations, and at most one call to a special function like the error function. The full derivation is given in the Appendix.

Finally, we integrate Equation (10) over projected separations D to obtain the total number of expected detections around an object, giving us $\langle N_{\rm obj}\rangle$ in Equation (7). We perform the integral using the trapezoidal rule in logarithmic separation, interpolating from the input contrast curves using cubic splines. Our use of cubic splines virtually guarantees the lack of a finite second derivative, irrespective of any intrinsic features of the contrast curves themselves, and makes the trapezoidal rule first order. We therefore use Richardson extrapolation with a fit linear in step size, and accept the result of the extrapolation when it agrees with the previous extrapolated result (using half as many function evaluations) within a factor of 3×10^{-3}. This tolerance allows relatively few function evaluations, while preventing the integration from dominating our error budget. It generally requires using ∼30–100 points in angular separation, at a cost of ∼0.05–0.1 ms per star on a single 3.3 GHz thread. Processing an entire large survey of 200 stars with a single set of test parameters thus requires about 10–20 ms, an enormous improvement over Monte Carlo methods that generate millions of planets around each star.

After evaluating $\langle N_{\rm obj}\rangle$ by integrating Equation (10) and summing over stars, we need to evaluate the probabilities λ_j of detectable companions existing at their observed positions D_j and luminosities L_j. Substellar companions are inevitably followed up many times, making the uncertainties on their luminosities very small. The photometric uncertainties are often dominated by scatter in the host star's photometry and variation in the AO performance across the field, bearing little relation to the annular standard deviation in the discovery image. The probabilities λ_j, taking the L_j as known, become

$$\lambda_j = p(\text{detect}|D_j, L_j)\left(\frac{dN}{d\ln L\,dD}d\ln L\,dD\right)\Big|_{D_j,L_j}\ . \tag{11}$$

This is equivalent to using Monte Carlo to find the number of companions in a small interval Δmag. The detection probability is a function only of L_j (which is observed). Because it is independent of the substellar distribution function, the detection probability contributes to an overall scaling of the likelihood function and has no effect on our analysis.

In practice, it is problematic to use Equation (11) as written because the derivative can be discontinuous or even, near the deuterium-burning limit, singular. We therefore integrate it over a small interval in $\ln L$:

$$\lambda_j \propto \int_{x_1}^{x_2} \frac{dN}{d\ln L\,dD}d\ln L\ , \tag{12}$$

We adopt 0.1 magnitudes (∼10% in luminosity) as our fiducial half-width $(x_2 - x_1)/2$, which is comparable to

the photometric errors on well-characterized companions like GJ 504b (Kuzuhara et al. 2013) and β Pictoris b (Bonnefoy et al. 2013). Though this width is somewhat arbitrary, we note that half-widths from 0.01 to 0.2 magnitudes give indistinguishable best-fit parameters and confidence intervals in our final analysis. Constant factors, like a variable increment in dD, do not affect our result; they merely add a constant to the log likelihood (equivalently, they multiply the likelihood by a constant).

All of the approximations and tabulations described above introduce errors of $\lesssim$1% (and substantially less for most parameter values of interest), which are smaller than those introduced by interpolating substellar cooling models in mass and age. The tabulated cooling models (Section 5) and stellar ages (Section 4) dominate the errors in our analysis.

6.2. *Model Constraints*

Our model for the exoplanet distribution function,

$$N(M, a) = AM^{\beta}a^{\alpha}, \tag{13}$$

with

$$a_{\min} < a < a_{\max} \quad \text{and} \quad M_{\min} < M < M_{\max}, \tag{14}$$

has seven free parameters, not counting the substellar cooling model:

1. The normalization of the distribution function, or, equivalently, the fraction of stars hosting substellar companions with a given range of properties;
2. α, the slope of the semimajor axis distribution function;
3. β, the slope of the mass distribution function;
4. $M_{\min}$, the minimum mass of the population;
5. $M_{\max}$, the maximum mass of the population;
6. $a_{\min}$, the inner edge of the semimajor axis distribution; and
7. $a_{\max}$, the outer edge of the semimajor axis distribution.

The normalization could also be a function of the host stellar mass, while $a_{\min}$ and $a_{\max}$ are both likely to scale with stellar mass (as might $M_{\min}$ and $M_{\max}$), which could add even more parameters.

Unfortunately, our sample contains far too few detections—κ And b, plus two brown dwarf companions in the Pleiades and two companions to NICI targets—to provide meaningful constraints on the full companion distribution function. Instead, we ask two much simpler questions:

- Out to what semimajor axis could the exoplanet distribution function measured by RV surveys extend?
- Can we use a single power law to describe the full population of objects from $\sim$5 M_J to massive brown dwarfs?

In this way, we attempt to address the question of whether the planets now being discovered by direct imaging represent a new population, distinct from both an extrapolation of the RV sample and of the more massive brown dwarfs.

Even addressing these more limited questions poses considerable difficulties. The distribution function of RV planets around solar-type FGK stars has been reasonably well-measured (Cumming et al. 2008); however, it depends both on stellar mass and on metallicity (Johnson et al. 2007a; Fischer & Valenti 2005). We lack metallicity data on many of our stars, and the sample, being largely young, spans a relatively narrow range in metallicity. We therefore make no attempt to take stellar enrichment into account. We do, however, attempt to at least qualitatively correct for host stellar mass, by assuming the planet-hosting probability to be directly proportional to the stellar mass in units of $M_{\odot}$ (a crude fit to the histogram presented in Johnson et al. 2007a). This fits with the observed correlation of disk mass with stellar mass (Andrews et al. 2013), though a correlation between stellar and companion *mass* may be a more natural choice. The latter is equivalent to using an upper limit of the mass distribution that depends on host stellar mass, and emphasizes the artificial nature of using a power law truncated at the deuterium burning limit.

The substellar cooling model appropriate to the RV population is hotly debated (see the discussion in Section 5). Objects formed by direct gravitational collapse do not have time to radiate away their heat of formation, while objects formed by core-accretion could lose much of their initial entropy in an accretion shock. We parametrize our ignorance using the SB12 warm-start models, using a variable warmth parameter $\eta \in [0, 1]$ to interpolate between the warmest and coldest starts for each mass. We also include the BT-Settl hot-start models (Allard et al. 2011), which apply over the entire range of masses from $\sim$1 M_J to the hydrogen burning limit.

For our fits to a brown-dwarf-like distribution, we set the limits on the semimajor axis distribution to be 1–1000 AU, well outside the regions typically probed around our targets, and set the lower mass cutoff to be 5 M_J, consistent with the minimum mass predicted by models of disk instability at wide separations (Rafikov 2005) and fragmentation in molecular clouds (Low & Lynden-Bell 1976; Bate et al. 2003). Unfortunately, the upper mass limit of this distribution is uncertain: the upper mass cutoff for disk fragmentation could differ from that for cloud fragmentation. However, our data lack the power to determine this cutoff, which we provisionally set at 70 M_J. A brown-dwarf like distribution is generally accepted to form by direct gravitational collapse. The hot-start BT-Settl models thus provide an appropriate benchmark to constrain the properties of this distribution.

Finally, we adopt uniform priors on α and β and reinterpret the likelihood function as an unnormalized posterior probability distribution. Using Monte Carlo to compute the normalization, we may then place constraints on α and β.

7. RESULTS AND DISCUSSION

Figure 1 shows the completeness of our data set given our age estimates and assuming either the hot-start BT-

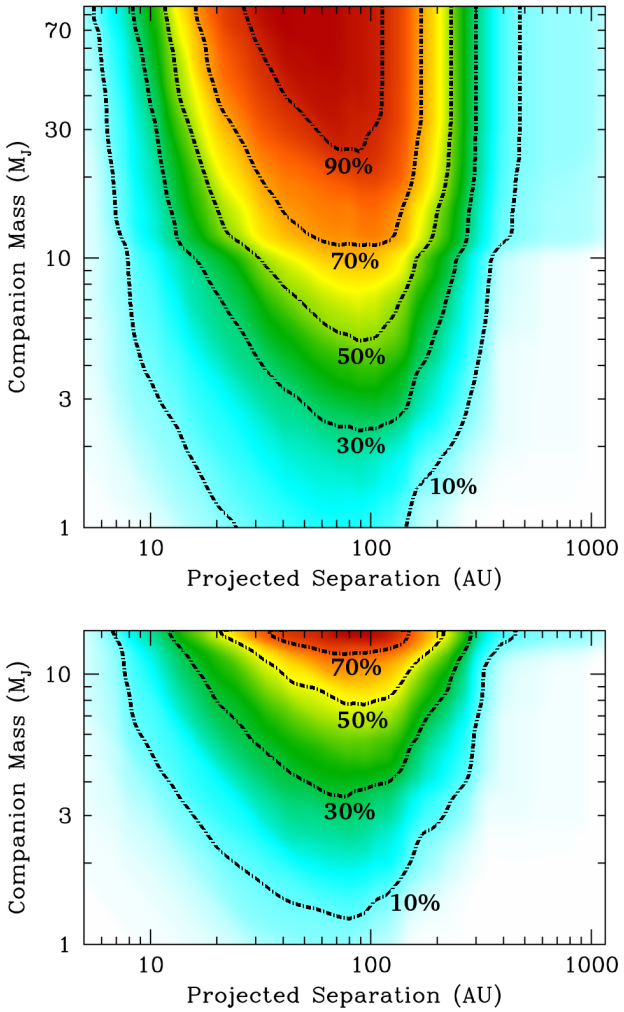

FIG. 1.— The completeness of our combined survey, calculated using the BT-Settl hot-start models (top panel) and a warm start model (initial entropy halfway between the hottest and coldest starts), and weighting all stars equally. At separations of 50–100 AU, we are about 70% complete at the deuterium burning threshold of ∼13 M_J under both models.

Settl cooling models (Allard et al. 2011), or a warm-start model (SB12) with an initial entropy halfway between the coldest and hottest starts ($\eta = 0.5$). At separations of 50–100 AU, we are sensitive to ∼60% of objects near the deuterium burning limit. This value is higher around stars closer to Earth, which tend to be of lower mass, and around stars reliably identified with a young MG.

In this section, we use the detection limits to determine the limits we can place on an extrapolation of the distribution function measured by radial velocities. We then proceed to model the entire substellar distribution function using a single power law, and determine its parameters and their confidence intervals.

7.1. *Limits on an RV Distribution Function*

The distribution function as measured by Cumming et al. (2008) follows $M^{-1.3}a^{-0.6}$ from 0.5 to 10 M_J and from 0.03 to 3 AU. We extrapolate this up to the deuterium burning limit of ∼13 M_J and out to a semimajor axis of a_{max}, which we seek to constrain. The normalization of the Cumming et al. distribution function is not free: 10.5% of 1 $M_\odot$ stars have a planet with a mass between 0.3 and 10 M_{Jup} and a semimajor axis between 0.03 and 3 AU. With the normalization fixed, we integrate Equation (10) over separations and sum over stars to get the expected number of detections, $\langle N_{obj} \rangle$. We then compare $\langle N_{obj} \rangle$ to the actual number of planet candidates in our sample using the Poisson distribution.

If an extrapolated RV planet distribution is to explain recent discoveries like GJ 504b, HR 8799b, κ And b, and HD 95086b, a_{max} must be $\gtrsim$50 AU, where these companions have been found. The sample we present here, depending on whether κ And b is hypothesized to arise from an RV-like distribution, has at most one detection in total, and zero around FGKM stars. If κ And b is more than ∼15 M_J, as would be the case if, as suggested by Hinkley et al. (2013) and Bonnefoy et al. (2014), it is older than the ∼30 Myr implied by membership in the Columba MG (Carson et al. 2013), we can exclude models that predict more than 3 detections with 95% confidence. If κ And b is considered to be a candidate member of an extrapolated RV distribution, the 2σ threshold rises to 4.7 predicted detections. We truncate the distribution at the deuterium burning threshold of 13 M_J for comparison to previous results and to facilitate the use of the SB12 models, which are only calculated for masses up to 15 M_J.

Figure 2 shows the predicted number of detections as a function of a_{max} for the BT-Settl model and for SB12 warm-start models spanning the range from hot to cold starts. For the BT-Settl hot start models, the 2σ upper limit on a_{max} varies from 30 to 50 AU, depending on whether we scale the companion frequency with stellar mass and whether we consider κ And b to arise from this distribution. If we adopt the SB12 models, the equivalent 2σ upper limits vary from 40 to 70 AU as long as we do not consider the very coldest start models (those with $\eta \lesssim 0.1$). If we do adopt these cold-start models, the upper limit on a_{max} rises to as much as ∼150 AU. We note that cold-start models would predict a mass for κ And b well in excess of the deuterium burning limit (Carson et al. 2013) and would justify that object's classification as a nonmember of this distribution, regardless of its membership in Columba.

Our finding that the RV distribution function of Cumming et al. (2008) cannot be extrapolated past a semimajor axis of ∼30–70 AU for most assumptions about the substellar cooling model is similar to the earlier results of Nielsen & Close (2010) and Chauvin et al. (2010). Nielsen & Close (2010) used a smaller sample of 118 targets dominated by the GDPS, finding limits on a_{max} from ∼65–200 AU depending on the substellar cooling model and on the correlation between planet frequency and stellar mass. Chauvin et al. (2010) used 88 young stars to constrain this outer limit to be ∼80 AU, again depending on the cooling model and the details of the distribution function. These results are in mild tension with the discovery of objects like HR 8799b, GJ 504b. and HD 95086b. which all lie at separations of $\gtrsim$50 AU. There may be even more tension with the form of the mass distribution, which in RV surveys, is a power law increasing sharply towards low masses. Wahhaj et al. (2013b) found a positive power law index for the distribution in planet mass (more massive objects are more common), in sharp disagreement from the RV findings. This result, how-

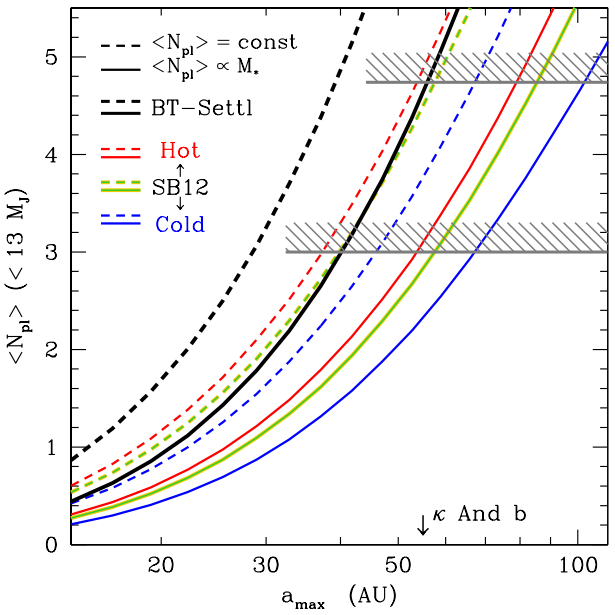

FIG. 2.— Expected number of planetary-mass detections as a function of semimajor axis cutoff and cooling model, computed by extrapolating the measured distribution function for RV planets (Cumming et al. 2008). The solid lines assume the number of companions to be proportional to host stellar mass, while the dashed lines assume no proportionality. The gray hatched regions are excluded at 2σ assuming κ And b to be drawn from this distribution (top, $\langle N_{\rm pl}\rangle \approx 4.7$), or to belong to a separate distribution (bottom, $\langle N_{\rm pl}\rangle \approx 3$)

ever, was driven by their inclusion of the four HR 8799 planets as independent detections and their lack of any detected companions $\lesssim$5 M_J. Excluding HR 8799 from the Wahhaj et al. (2013b) analysis weakens this finding considerably.

7.2. *A Single Substellar Distribution Function*

The preceding analysis artificially separates objects below and above the deuterium burning threshold, making the classification of substellar companions like κ And b problematic. It also does not consider the properties of the detected companions. We now consider a distribution function extending across the deuterium-burning threshold, up to the hydrogen burning limit of $\sim$70 $M_{\rm Jup}$. The predicted probability density of detections may be projected onto substellar mass and semimajor axis, and compared with our sample. For this exercise, and for the statistical analysis that follows, we add two additional substellar companions discovered by HiCIAO: GJ 758B (Thalmann et al. 2009; Janson et al. 2011), a $\sim$30 M_J brown dwarf around an old G star first imaged during HiCIAO commissioning, and GJ 504b (Kuzuhara et al. 2013; Janson et al. 2013a), a $\sim$3–8 M_J companion to an active field G star discovered during the full SEEDS survey. By doing this, we assume that the contrasts, distances, and ages of the as-yet-unpublished HiCIAO data are similar to those presented in Section 3. In reality, the unpublished stars stars represent a combination of very young members of starforming regions and nearby stars with a wide range of ages, a heterogeneity to that of our combined sample.

We first show the predictions of two published distribution functions: $dN/dMda \propto M^{-0.4}a^{-1}$, derived for both stellar and substellar companions from $\sim$30–1500 AU (Metchev & Hillenbrand 2009), and $dN/dMda \propto M^{-1.3}a^{-0.6}$, derived for $\sim$1–10 $M_{\rm Jup}$ RV-detected companions from $\sim$0.03–3 AU (Cumming et al. 2008). In the former case, we extend the distribution down to 1 $M_{\rm Jup}$ and out to 1000 AU, well outside the field-of-view around nearly all of our targets. In the latter case, we extrapolate the distribution function up to the hydrogen burning limit of $\sim$70 $M_{\rm Jup}$ and out to 100 AU, roughly the outermost semimajor axis consistent with our analysis in Section 7.1, and scale companion frequency with stellar mass. Figure 3 shows the predicted probability densities, $dp/d\log M/d\log D$, for both of these distributions, together with contours of constant $dp/d\log M/d\log D$ enclosing 68% and 95% of the predicted detections. The five HiCIAO detections, including GJ 504b and GJ 758B, are in red, while the two NICI detections are shown in green.

The Metchev & Hillenbrand (2009) distribution, the top panel in Figure 3, appears to provide a reasonably good fit to our sample, though it has some difficulty accounting for objects like GJ 504b (depending on its age). The inclusion of intermediate separation low-mass companions from other surveys, like HD 95086b (which was discovered in a survey that did not detect any massive brown dwarfs), or of β Pic b and HR 8799bcde, would add to this tension. The RV-inspired distribution, bottom panel of Figure 3, terminates at 100 AU and is unable to account for the massive ($\sim$60 M_J), long-period brown dwarfs discovered in the Pleiades. We note that the distribution advocated by Zuckerman & Song (2009), with $p(M,a) \propto M^{-1.2}a^{-1}$ (not shown), has a nearly identical mass dependence but extends to larger semimajor axes. This distribution can accommodate all of the detections, though only if we extend it well below the $\sim$12 $M_{\rm Jup}$ limit suggested by Zuckerman & Song in order to match GJ 504b.

We now return to our sample, using our detections and contrast curves to constrain the substellar distribution function. Given an assumed form of the distribution function, including the power law indices and mass and semimajor axis limits, we may then use the likelihood function (in the form of Equation (7)) to compare the distribution to our actual detections. We assume uniform priors on the power law indices α and β, integrate the likelihood function, and treat it as a posterior probability distribution. The additional effect of including GJ 504b and GJ 758B in a full analysis may be crudely estimated by scaling up our sample size to qualitatively account for the as-yet-unpublished non-detections. Such a scaling would simply multiply $\langle N_{\rm obj}\rangle$ in Equation (7) by a constant, dropping out when constraining α and β. This implicitly assumes that the ages, distances, and masses probed by the as-yet-unpublished non-detections are similar to those of the sample presented here. Given the heterogeneity of both our combined sample and the unpublished SEEDS data, this is not a bad approximation. We set $a_{\rm min} = 1$ AU and $a_{\rm max} = 1000$ AU, well outside the regions of interest, and use a lower mass cutoff of 5 M_J, appropriate to a gravitational collapse scenario.

Including all of the detections in our merged sample, and adding GJ 504b and GJ 758B. we obtain a best-fit

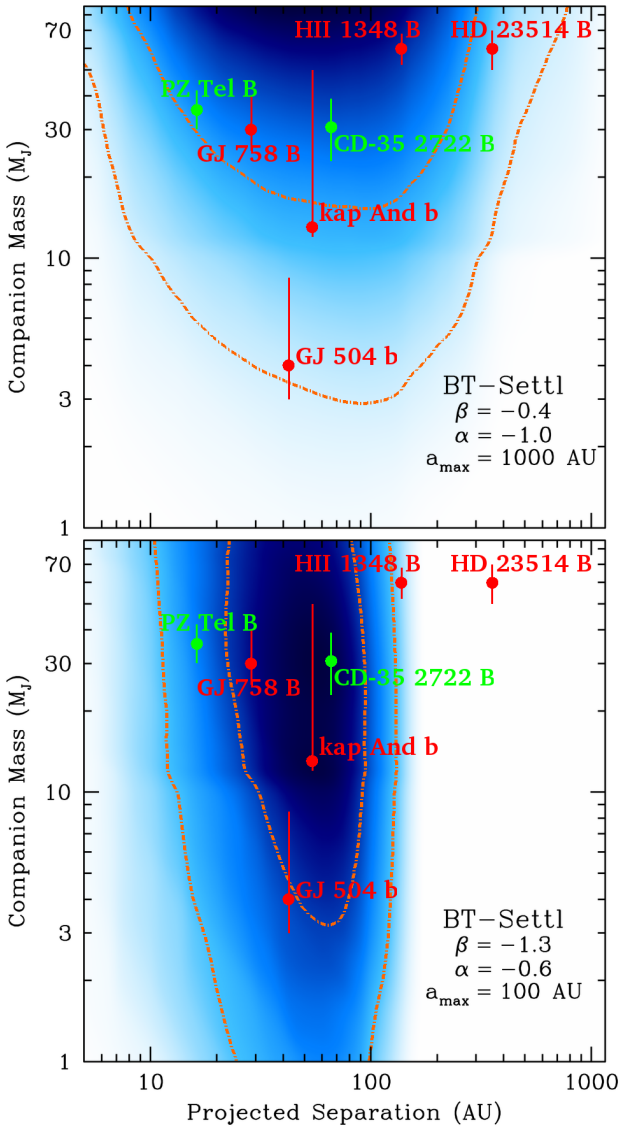

FIG. 3.— Probability distributions, $dp/d\log M/d\log D$, under two different substellar distribution functions, $p(M,a) \propto a^{\alpha} M^{\beta}$. NICI discoveries are shown in green; companions imaged by Hi-CIAO are shown in red. The distribution with $\beta = -0.4$, (top panel, taken from Metchev & Hillenbrand 2009), predicts a large number of massive brown dwarfs at separations of ∼50–100 AU. The bottom distribution is that published in Cumming et al. (2008), with $\alpha = -0.6$ and $\beta = -1.3$, extrapolated out to higher masses and semimajor axes, and assuming planet frequency to scale with host stellar mass. The massive Pleiades brown dwarfs, H II 1348B and HD 23514B. would force the outer limit to extend to ∼300 AU, which is excluded by our sample (Figure 2). They cannot arise from an extrapolation of the RV distribution function.

distribution function $p(M,a) \propto M^{-0.65\pm0.60} a^{-0.85\pm0.39}$ (1σ errors). Abandoning the lower limit on companion mass favors a distribution function with somewhat more high-mass objects, with the mass exponent becoming -0.4 ± 0.5 (1σ errors). However, as discussed in Section 2, there are theoretical reasons to impose such a lower mass limit for gravitational collapse, and a cutoff is also suggested by the dearth of companions <5 M_J in other high-contrast surveys.

The normalization of the distribution function is given by a gamma distribution at fixed α and β; its maximum likelihood value produces five detections (the observed number) in our sample of 248 stars. With $(\alpha, \beta) = (-0.85, -0.65)$, the maximum likelihood normalization constant gives 1.7% of stars with substellar companions between 5 and 70 $M_{\rm Jup}$ and between 10 and 100 AU. The gamma distribution is asymmetric; the 68% and 95% confidence intervals are 1.2–2.8% and 0.74–3.9%, respectively, of stars with companions in the given mass and semimajor axis range. If we also include uncertainty in α and β by integrating the likelihood function and treating it as a posterior distribution, the uncertainty in the normalization constant increases somewhat. For companions between 5 and 70 $M_{\rm Jup}$ and between 10 and 100 AU, the 68% and 95% confidence intervals become 1.0–3.1% and 0.52–4.9% of stars, respectively.

We also extrapolate our distribution out to $a = 1600$ AU to facilitate comparison with Metchev & Hillenbrand (2009), again using both the gamma distribution and uncertainties in α and β to derive the full probability distribution of the fraction of stars hosting companions. We find that, at 68% confidence, 1.8–6.2% of stars host brown dwarfs between 12 and 72 $M_{\rm Jup}$ and between 28 and 1600 AU (0.92–11% at 95% confidence). These results agree very well with the Metchev & Hillenbrand value of $3.2^{+3.1}_{-2.7}$% (2σ limits). The latter analysis fixed $\alpha = -1$ and assumed a continuous mass function extending to stellar companions, making the agreement particularly gratifying. Omitting the uncertainty in α and β, our results imply that 1.4–7.2% of stars host 12–72 $M_{\rm Jup}$ with semimajor axes from 28–1600 AU at 95% confidence.

The results from many other surveys in the H and K bands would fit nicely on Figure 4, and further suggest a smooth distribution across the deuterium burning threshold. Chauvin et al. (2010) reported the detection of three substellar objects in their survey, of which two, GSC-08047-00232B (Chauvin et al. 2005a), and AB Pic b (Chauvin et al. 2005b), are ∼20 and ∼15 M_J brown dwarf companions 250–300 AU from their host stars. These data suggest that a smooth distribution extending all the way from massive brown dwarfs down to a theoretically motivated cutoff at ∼5 M_J is capable of explaining the vast majority of wide-separation companions below or near the deuterium-burning limit nominally separating planets from brown dwarfs.

7.3. *Limitations*

Our statistical analysis makes several assumptions that are not true in detail. For example, we do not distinguish between single stars and binaries (which make up a relatively small fraction of our sample, ∼10%). Some orbits are unstable around binaries (Holman & Wiegert 1999); however, simply excluding these regions of parameter space and considering the rest other orbits to be as probable as around a single star is not a well-motivated solution. Low-mass companions could be scattered to distant orbits by a close stellar binary, possibly making binaries better systems to find substellar objects. In most cases, the orbital elements of the stellar binary are unknown anyway. We therefore accept that our neglect of binarity might introduce a modest bias, but we lack a good solution other than excluding binaries altogether.

Our analysis also neglects sample biases, which can appear in many ways. Stars hosting debris disks may be more likely to harbor planets. Treating them identi-

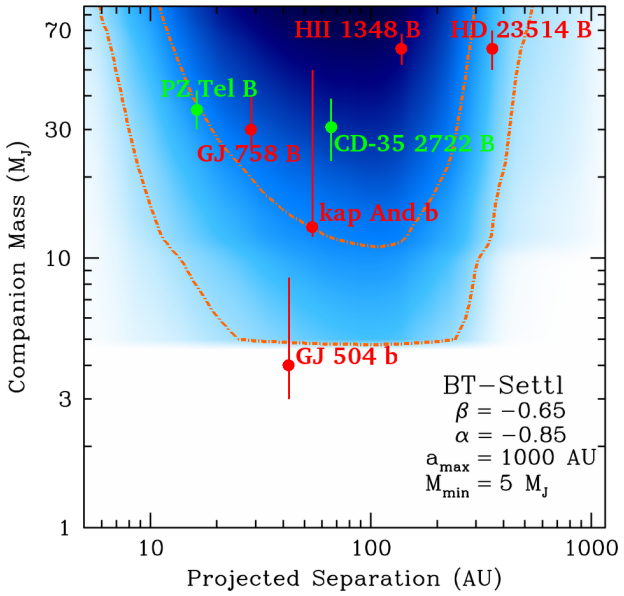

FIG. 4.— The probability distribution, $dp/d\log M/d\log D$, for the maximum likelihood power law distribution including all seven detections shown: $p(M,a) \propto M^{-0.65\pm0.60}a^{-0.85\pm0.39}$ (1σ errors). NICI discoveries are in green, while companions imaged by Hi-CIAO are in red. This result should be interpreted with caution, but is compatible with the distributions published in both Metchev & Hillenbrand (2009) and Zuckerman & Song (2009) within 1σ. It suggests that we cannot reject a single substellar distribution function extending from massive brown dwarfs to massive exoplanets based solely on the sample presented here.

cally to stars without infrared excesses, as we do here, could artificially depress the derived planet frequency. SEEDS also avoided including known planet hosts and attempted to avoid observing stars targeted by other high-contrast instruments. A tendency to avoid observing the same targets as other surveys, but to repeat some targets around which nothing was found, would likewise bias us against finding planets.

The choice of substellar cooling model introduces another opportunity for bias, as we discuss in Section 5. This is somewhat mitigated for our sample by the wide range of ages we probe, and by the fact that the luminosity of a brown dwarf or exoplanet depends so strongly on its mass and age. Particularly for objects formed by direct gravitational collapse, there is little doubt about the initial thermodynamic state, though systematic errors could still arise from, e.g., a poor treatment of cloud formation.

Possibly the most serious limitation of our analysis comes from our ignorance of the formation mechanism of substellar objects, and our resulting assumption of separable power law distribution functions. Substellar objects do not form in isolation; many have been imaged around stellar binaries. These objects would interact dynamically with other stars or brown dwarfs, with lighter companions being preferentially scattered outwards, and more massive companions scattered inwards. As a result, the initial and final companion mass distributions may be very different from one another. Models of brown dwarf formation (e.g. Stamatellos & Whitworth 2009; Bate 2009) are beginning to predict distribution functions, but have difficulty producing low-mass brown dwarfs at moderate separations. As a result, we have little choice but to proceed with simplistic models based only loosely on theoretical considerations.

In addition to these limitations, there are several objects not included in our sample that may be difficult to incorporate into a single substellar distribution like the one suggested in Section 7.2, and that may represent the high-mass, wide-separation tail of a core-accretion population. These objects, including HR 8799bcde, β Pic b, and HD 95086b. tend to occur around relatively massive A-type stars. A stars rotate very rapidly and are therefore poor targets for radial velocity searches, making the application of a distribution function like that measured by Cumming et al. (2008) (used in Section 7.1) an extrapolation in both separation and host stellar mass. The masses of β Pic b and at least some of the HR 8799 planets have been dynamically constrained to be $\lesssim$10 M_J (Lagrange et al. 2012; Dawson et al. 2011; Sudol & Haghighipour 2012). Such low-mass companions at $\sim$10–40 AU are difficult to form in-situ by direct gravitational collapse (Rafikov 2005; Kratter et al. 2010), while some recent studies have found that core-accretion may be viable out to a few tens of AU (Lambrechts & Johansen 2012; Kenyon & Bromley 2009). Planet-planet scattering and migration do add some uncertainty to this picture.

As more low-mass companions are discovered, they may reveal a clear bimodal distribution in planet/star mass ratio, hints of which were shown by Currie et al. (2011). Such a clear separation would be strong evidence of different formation mechanisms. Even stronger evidence would be planetary chemical compositions differing strongly from those of their host stars. Konopacky et al. (2013) found signs of an enhanced C/O ratio in HR 8799c, though these results depend on chemical modeling of the atmosphere and were at modest significance. A bimodal distribution of metal and/or carbon enhancements, with a strong correlation between composition, separation, and mass ratio, would probably be conclusive. New and upcoming instruments like GPI (Macintosh et al. 2008), SPHERE (Beuzit et al. 2008), and CHARIS (Peters et al. 2012) may be able to provide these data over the next few years.

8. CONCLUSIONS

In this work, we present an analysis of high-contrast imaging of nearly 250 stars. The targets span a wide range of spectral types and ages, and are composed of three published subsets of the SEEDS survey on the Subaru telescope, combined with the GDPS and the NICI MG sample. We perform a uniform, Bayesian analysis of the ages of all of our targets, with determinations that are often more conservative than those adopted in previous papers. Our sample includes five detected substellar companions. Two of these are $\sim$60 M_J brown dwarfs around stars in the Pleiades; the others are a $\sim$13–50 M_J companion to the late B star κ And, a $\sim$35 M_J companion to the late G star PZ Tel, and a $\sim$30 M_J companion to the early M star CD−35 2722.

Our analysis includes a new method for calculating the likelihood function of a substellar distribution function by performing integrals analytically or evaluating them from tables whenever possible. This represents a large improvement in efficiency over using Monte Carlo to evaluate completeness, and allows us to efficiently compute

the likelihood of a wide range of models. We use these techniques to compute the limits beyond which the distribution function measured for RV planets cannot be extended, finding a model-dependent maximum semimajor axis limit of ∼30–100 AU, similar to previous results. However, we argue that the division of substellar objects at the deuterium burning limit is arbitrary, particularly in light of new discoveries that straddle that boundary, and we seek to model the entire substellar population using a single distribution function.

Finally, we use Monte Carlo to compute the likelihood function of a unified substellar distribution function, including the five companions detected in our sample, plus an additional two objects, GJ 758B. and GJ 504b. discovered by HiCIAO, for a total of seven. The inclusion of these objects does not bias the results as long as the distributions of target stars and contrast curves presented here are good matches to those of the unpublished nondetections from which GJ 758 and GJ 504 were culled. Given the wide range of stellar properties and ages in both samples, this is a fairly good assumption. With this caveat, we find that a single, separable power law, $p(M, a) \propto M^{-0.65\pm0.60} a^{-0.85\pm0.39}$ (1σ errors), truncated at a theoretically motivated minimum mass of ∼5 M_J, can account for the entire range of substellar companions detected in SEEDS. The normalization of this distribution implies that, at 68% confidence, 1.0–3.1% of stars have substellar companions between 5 and 70 $M_{\rm Jup}$ and between 10 and 100 AU (0.52–4.9% at 95% confidence). Extrapolating to larger separations, 1.8–6.2% of stars (at 68% confidence) have companions between 12 and 72 $M_{\rm Jup}$ and between 28 and 1600 AU (the limits used by Metchev & Hillenbrand 2009); or 0.92–11% at 95% confidence. Our normalization is in excellent agreement with the Metchev & Hillenbrand (2009) result, that $3.2^{+3.1}_{-2.7}$% (2σ limits) of stars have brown dwarf companions within these limits.

Our results suggest that many, perhaps most, of the substellar companions currently being discovered near and somewhat below the deuterium burning limit may share a common origin with more massive brown dwarfs. Such objects would almost certainly form by gravitational collapse, either in a disk or in a fragmenting cloud. There is currently little reason to consider the substellar companions, at least in our combined sample, to be the high-mass, long-period tail of the RV planet distribution.

Upcoming surveys using instruments like GPI (Macintosh et al. 2008), SPHERE (Beuzit et al. 2008), and CHARIS (Peters et al. 2012) will dramatically improve our sensitivity to low-mass companions, a region of parameter space that should be richly populated if current detections are described by an RV-like distribution function. The discovery of many such objects, below the mass limits at which clouds and disks are expected to fragment, could point to an alternative formation scenario, like core-accretion followed by dynamical evolution. If, however, such objects turn out to be exceptionally rare, the current population of directly imaged exoplanets likely represents the low-mass tail of the brown dwarfs.

This research is based on data collected at the Subaru Telescope, which is operated by the National Astronomical Observatories of Japan. TDB gratefully acknowledges support from the Corning Glass Works Foundation through a fellowship at the Institute for Advanced Study. This research has been supported in part by the World Premier International Research Center Initiative, MEXT, Japan. MK acknowledges support from a JSPS Research Fellowship for Young Scientists (grant No. 25-8826). JC was supported by the U.S. National Science Foundation under Award No. 1009203. This research has made use of the SIMBAD database and Vizier service, operated at CDS, Strasbourg, France. The authors wish to recognize and acknowledge the very significant cultural role and reverence that the summit of Mauna Kea has always had within the indigenous Hawaiian community. We are most fortunate to have the opportunity to conduct observations from this mountain.

APPENDIX

PROJECTED SEPARATION DISTRIBUTION FUNCTION

Denoting the projected separation (in physical units) as D, and the ratio of the projected distance to the semimajor axis by $s \in [0, 2]$, the probabillity distribution of D is

$$p(D) = \int_{s_1}^{s_2} ds\, p(s)\, p\left(a = \frac{D}{s}\right) \frac{1}{s}\ , \tag{A1}$$

where the last factor $1/s$ accounts for the volume element. If $p(a)$ is a power law a^α, truncated at $a_{\rm min}$ and $a_{\rm max}$, we have $s_1 = \min(2, D/a_{\rm max})$ and $s_2 = \min(2, D/a_{\rm min})$. In the special case that the power law is truncated well outside the separations of interest, $s_1 \approx 0$ and $s_2 \approx 2$, and the dependence of $p(D)$ on the eccentricity distribution drops out altogether.

We can empirically derive $p(s)$ from $p(e)$ using the method described in the appendix of Brandeker et al. (2006). This method assumes only that companions are observed at random times in their orbits and that their orbits are randomly oriented as seen from Earth. Brandeker et al. suggest an eccentricity distribution $p(e) = 2e$, the theoretical distribution expected if the phase space density of companions is a function of energy only (Ambartsumian 1937). However, planet-planet scattering disfavors eccentricities close to 1, producing distributions closer to the Rayleigh distribution with $\sigma \sim 0.3$ (Jurić & Tremaine 2008). Other authors (Cumming et al. 2008) have suggested a uniform distribution in eccentricity out to $e_{\rm max} \sim 0.8$. We adopt the latter distribution, noting, however, that a Rayleigh distribution with $\sigma = 0.3$ produces nearly indistinguishable results.

The top panel of Figure 5 shows all three distributions in s. The uniform distribution up to an eccentricity of 0.8 is

well-fit by a piecewise linear function:

$$p(s) \approx \begin{cases} 1.3s & 0 \le s \le 1 \\ -\frac{35}{32}\left(s - \frac{9}{5}\right) & 1 < s < 1.8 \end{cases} \tag{A2}$$

Assuming $p(a) = a^\alpha$ for $a_{\rm min} \le a \le a_{\rm max}$, we then perform the integral

$$p(D) = \int_{s_1}^{s_2} ds\, p(s)\, p\left(a = \frac{D}{s}\right) \frac{1}{s} \ , \tag{A3}$$

with $s_1 = \min(D/a_{\rm max}, 1.8)$ and $s_2 = \min(D/a_{\rm min}, 1.8)$. We have, after a bit of algebra,

$$p(D) = \begin{cases} D\left[\dfrac{1.3}{1-\alpha}\left(a_{\rm min}^{\alpha-1} - a_{\rm max}^{\alpha-1}\right)\right] & D < a_{\rm min} \\ D^\alpha\left[\dfrac{315+68\alpha}{160\alpha(1-\alpha)}\right] - D\left[\dfrac{1.3}{1-\alpha}a_{\rm max}^{\alpha-1} + \dfrac{35}{32(1-\alpha)}a_{\rm min}^{\alpha-1}\right] - \dfrac{63}{32\alpha}a_{\rm min}^\alpha & a_{\rm min} \le D < 1.8a_{\rm min} \\ D^\alpha\left[\dfrac{68\alpha + 315(1-1.8^{-\alpha})}{160\alpha(1-\alpha)}\right] - D\left[\dfrac{1.3}{1-\alpha}a_{\rm max}^{\alpha-1}\right] & 1.8a_{\rm min} \le D < a_{\rm max} \\ D^\alpha\left[-\dfrac{35}{32}\dfrac{1.8^{1-\alpha}}{\alpha(1-\alpha)}\right] + D\left[\dfrac{35}{32}\dfrac{a_{\rm max}^{\alpha-1}}{1-\alpha}\right] + \dfrac{63}{32\alpha}a_{\rm max}^\alpha & a_{\rm max} \le D \le 1.8a_{\rm max} \end{cases} \tag{A4}$$

Given $a_{\rm min}$, $a_{\rm max}$, and α, Equation (A4) is a sum of piecewise power laws, and is trivial to integrate analytically. The bottom panel of Figure 5 shows the final distributions $p(D)$ for each of the eccentricity distributions we consider, together with the piecewise analytic approximation given by Equation (A4). The blue and green curves, representing the exact result and our approximation, are nearly indistinguishable from one another and from the Rayleigh distribution (red curve).

For completeness, we also work out the case of an eccentricity distribution with

$$p(e) = 2e \ , \tag{A5}$$

the result obtained assuming the phase space density to be a function only of orbital energy. In this case, we can very closely approximate $p(s)$ by

$$p(s) \approx \frac{3}{4}\left(2s - s^2\right) \ . \tag{A6}$$

In their paper, Brandeker et al. (2006) used a sine curve, which provides a slightly worse fit and is much more difficult to handle analytically. With our approximation, the distribution $p(D)$ becomes

$$p(D) = D^\alpha\left[\frac{3}{2(1-\alpha)}\left(s_2^{1-\alpha} - s_1^{1-\alpha}\right) - \frac{3}{4(2-\alpha)}\left(s_2^{2-\alpha} - s_1^{2-\alpha}\right)\right] \ , \tag{A7}$$

with $s_1 = \min(D/a_{\rm max}, 2)$ and $s_2 = \min(D/a_{\rm min}, 2)$.

DETECTIONS AT A GIVEN SEPARATION

Suppose that the noise at angular separation D is σ_D, and the formal detection threshold is $L_{\rm lim} = N_\sigma \sigma_D$. The probability of detecting a companion of luminosity L, assuming Gaussian errors, is then

$$p({\rm detect}|L) = \frac{1}{2} + \frac{1}{2}{\rm erf}\left(\frac{N_\sigma(L - L_{\rm lim})}{L_{\rm lim}\sqrt{2}}\right) \ , \tag{B1}$$

where erf is the error function. The total number of detected companions at angular separation D is then

$$N(D) = \int_0^\infty \frac{dN}{dL} p({\rm detect}|L)\, dL = \int_0^\infty \frac{dN}{dM}\frac{dM}{dL} p({\rm detect}|L)\, dL \ . \tag{B2}$$

Substellar cooling models are generally presented as grids in mass-luminosity space, which we interpolate using piecewise power laws, with

$$\frac{L}{L_i} = \left(\frac{M}{M_i}\right)^{\gamma_i} \tag{B3}$$

for $M_{i,0} \le M < M_{i,1}$ or, equivalently, for $L_{i,0} \le L < L_{i,1}$. Defining

$$x \equiv \frac{L}{L_{\rm lim}} \ \ {\rm and} \ \ \Gamma_i \equiv (\beta + 1 - \gamma_i)/\gamma_i \ , \tag{B4}$$

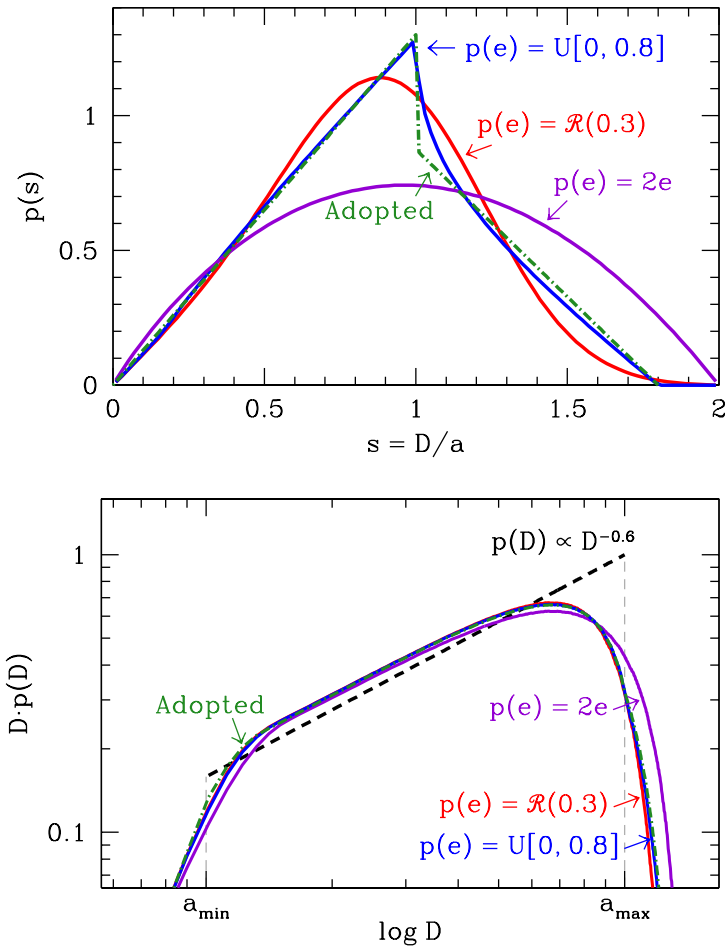

FIG. 5.— Top panel: the distribution of $s = D/a$ assuming the eccentricity to be uniformly distributed between 0 and 0.8 (blue curve), Rayleigh distributed with $\sigma = 0.3$ (red curve), or with $p(e) = 2e$ (violet curve). We adopt the piecewise linear approximation represented by the green curve. Bottom panel: the distributions of projected separation produced by a truncated power law distribution in semimajor axis (black curve) for each distribution in s from the top panel. We use the piecewise analytic green dot-dashed curve, which is nearly identical to the results from the Rayleigh and uniform distributions; we also provide an expression that is nearly indistinguishable from the violet curve.

and assuming the distribution function of mass to be

$$p_M(M) \propto M^\beta \ , \tag{B5}$$

we have, after some algebra,

$$N(D) = \sum_i M_i p_M(M_i) \int_{x_{i,0}}^{x_{i,1}} \frac{1}{\gamma_i} x^{\Gamma_i} \left[\frac{1}{2} + \frac{1}{2}\mathrm{erf}\left(\frac{(x-1)N_\sigma}{\sqrt{2}}\right)\right] dx \ . \tag{B6}$$

The integral in Equation (B6) is a function only of the limits of integration and of the quantity $\Gamma_i = (\beta + 1 - \gamma_i)/\gamma_i$. We approximate the integral in different regimes depending on the values of $x_{i,0}$, $x_{i,1}$, and γ_i. For $5 \le N_\sigma \le 6$, $x = 0.4$ corresponds to 3–4σ below the formal detection limit, while $x = 1.6$ is 3–4σ above the formal detection limit. We adopt the following approximations:

1. $x_{i,1} < 0.4$: The integral is nearly zero.

2. $x_{i,1} > 0.4$ and $\Gamma \notin [-6, 10]$: For $\beta \in [-3, 2]$ (ranging from exceptionally bottom heavy to exceptionally top-heavy; $\beta \sim -1$ from RV studies), this would imply $\gamma < 1/3$, i.e., the dependence of luminosity of mass is exceptionally weak. We approximate the error function as a constant, obtaining

$$\frac{1}{\beta+1}\left(M_{i,1}p_M(M_{i,1}) - M_{i,0}p_M(M_{i,0})\right)\left[\frac{1}{2} + \frac{1}{2}\mathrm{erf}\left(\frac{(L_i/L_{\rm lim} - 1)\,N_\sigma}{\sqrt{2}}\right)\right] \ . \tag{B7}$$

3. $0.4 < x_{i,1} < 1.6$ and $-6 \le \Gamma \le 10$: We evaluate the integral from tabulated quadratic fits. We set the lower limit of integration to $\min(0.4, x_{i,0})$.

4. $x_{i,1} > 1.6$ and $-6 \leq \Gamma \leq 10$: We evaluate the integral from tabulated quadratic fits, setting the lower limit of integration to $\min(0.4,\, x_{i,0})$ and the upper limit to 1.6. We then integrate the entire rest of the mass distribution (assuming a nearly monotonic mass-luminosity relation), obtaining

$$\frac{1}{\beta+1}\left[M_{\max}p_M(M_{\max}) - M_i p_M(M_i)\left(\frac{1.6L_{\lim}}{L_i}\right)^{(\beta+1)/\gamma_i}\right] . \tag{B8}$$

Assuming we pre-compute p_M at the tabulated masses, each of these approximations requires at most one call to a special function (power or erf), a handful of array lookups, and ∼20 floating point operations. Our tabulated fits to the integrals are always accurate to better than 0.1% of the integral evaluated between $x = 0.4$ and 1.6; these approximations therefore introduce less error than the (inevitable) interpolations over the grid of models.

REFERENCES

Alibert, Y., Mordasini, C., Benz, W., & Winisdoerffer, C. 2005, A&A, 434, 343
Allard, F., Hauschildt, P. H., Alexander, D. R., Tamanai, A., & Schweitzer, A. 2001, ApJ, 556, 357
Allard, F., Homeier, D., & Freytag, B. 2011, in Astronomical Society of the Pacific Conference Series, Vol. 448, 16th Cambridge Workshop on Cool Stars, Stellar Systems, and the Sun, ed. C. Johns-Krull, M. K. Browning, & A. A. West, 91
Ambartsumian, V. A. 1937, Astron. Zhurn., 14, 207
An, D., Terndrup, D. M., Pinsonneault, M. H., et al. 2007, ApJ, 655, 233
Andrews, S. M., Rosenfeld, K. A., Kraus, A. L., & Wilner, D. J. 2013, ApJ, 771, 129
Bakos, G., Noyes, R. W., Kovács, G., et al. 2004, PASP, 116, 266
Baliunas, S. L., Donahue, R. A., Soon, W. H., et al. 1995, ApJ, 438, 269
Baraffe, I., Chabrier, G., Barman, T. S., Allard, F., & Hauschildt, P. H. 2003, A&A, 402, 701
Batalha, N. M., Rowe, J. F., Bryson, S. T., et al. 2013, ApJS, 204, 24
Bate, M. R. 2009, MNRAS, 392, 590
Bate, M. R., Bonnell, I. A., & Bromm, V. 2002, MNRAS, 332, L65
Bate, M. R., Bonnell, I. A., & Bromm, V. 2003, MNRAS, 339, 577
Beuzit, J.-L., Feldt, M., Dohlen, K., et al. 2008, in Society of Photo-Optical Instrumentation Engineers (SPIE) Conference Series, Vol. 7014, Society of Photo-Optical Instrumentation Engineers (SPIE) Conference Series
Biller, B. A., Liu, M. C., Wahhaj, Z., et al. 2010, ApJ, 720, L82
Biller, B. A., Liu, M. C., Wahhaj, Z., et al. 2013, ApJ, 777, 160
Binks, A. S., & Jeffries, R. D. 2014, MNRAS, 438, L11
Boley, A. C. 2009, ApJ, 695, L53
Bonfils, X., Delfosse, X., Udry, S., et al. 2013, A&A, 549, A109
Bonnefoy, M., Boccaletti, A., Lagrange, A.-M., et al. 2013, A&A, 555, A107
Bonnefoy, M., Currie, T., Marleau, G.-D., et al. 2014, A&A, 562, A111
Boss, A. P. 1997, Science, 276, 1836
Boss, A. P. 2000, ApJ, 536, L101
Bowler, B. P., Liu, M. C., Shkolnik, E. L., & Dupuy, T. J. 2013, ArXiv e-prints, 1307.2237
Brandeker, A., Jayawardhana, R., Khavari, P., Haisch, K. E., Jr., & Mardones, D. 2006, ApJ, 652, 1572
Brandt, T. D., Kuzuhara, M., McElwain, M. W., et al. 2014, ApJ, 786, 1
Brandt, T. D., McElwain, M. W., Turner, E. L., et al. 2013, ApJ, 764, 183
Bromley, B. C., & Kenyon, S. J. 2011, ApJ, 731, 101
Carson, J., Thalmann, C., Janson, M., et al. 2013, ApJ, 763, L32
Chabrier, G. 2003, PASP, 115, 763
Chabrier, G., Baraffe, I., Allard, F., & Hauschildt, P. 2000, ApJ, 542, 464
Chauvin, G., Lagrange, A.-M., Bonavita, M., et al. 2010, A&A, 509, A52
Chauvin, G., Lagrange, A.-M., Lacombe, F., et al. 2005a, A&A, 430, 1027
Chauvin, G., Lagrange, A.-M., Zuckerman, B., et al. 2005b, A&A, 438, L29
Chauvin, G., Vigan, A., Bonnefoy, M., et al. 2014, ArXiv e-prints, 1405.1560
Chen, C. H., Mamajek, E. E., Bitner, M. A., et al. 2011, ApJ, 738, 122
Chen, C. H., Sargent, B. A., Bohac, C., et al. 2006, ApJS, 166, 351
Craig, N., Christian, D. J., Dupuis, J., & Roberts, B. A. 1997, AJ, 114, 244
Cumming, A., Butler, R. P., Marcy, G. W., et al. 2008, PASP, 120, 531
Currie, T., Burrows, A., Itoh, Y., et al. 2011, ApJ, 729, 128
Currie, T., Daemgen, S., Debes, J., et al. 2014, ApJ, 780, L30
Currie, T., Debes, J., Rodigas, T. J., et al. 2012, ApJ, 760, L32
da Silva, L., Torres, C. A. O., de La Reza, R., et al. 2009, A&A, 508, 833
Dawson, R. I., Murray-Clay, R. A., & Fabrycky, D. C. 2011, ApJ, 743, L17
de Zeeuw, P. T., Hoogerwerf, R., de Bruijne, J. H. J., Brown, A. G. A., & Blaauw, A. 1999, AJ, 117, 354
Delfosse, X., Forveille, T., Mayor, M., et al. 1998, A&A, 338, L67
Delorme, P., Gagné, J., Girard, J. H., et al. 2013, ArXiv e-prints, 1303.4525
Dodson-Robinson, S. E., Veras, D., Ford, E. B., & Beichman, C. A. 2009, ApJ, 707, 79
Duquennoy, A., & Mayor, M. 1991, A&A, 248, 485
Eiroa, C., Marshall, J. P., Mora, A., et al. 2011, A&A, 536, L4
Fernández, D., Figueras, F., & Torra, J. 2008, A&A, 480, 735
Fischer, D. A., & Valenti, J. 2005, ApJ, 622, 1102
Gagné, J., Lafrenière, D., Doyon, R., Malo, L., & Artigau, É. 2014, ApJ, 783, 121
Gaidos, E. J., Henry, G. W., & Henry, S. M. 2000, AJ, 120, 1006
Geißler, K., Metchev, S. A., Pham, A., et al. 2012, ApJ, 746, 44
Ghezzi, L., Cunha, K., Smith, V. V., et al. 2010, ApJ, 720, 1290
Gizis, J. E., Kirkpatrick, J. D., Burgasser, A., et al. 2001, ApJ, 551, L163
Głębocki, R., & Gnaciński, P. 2005, in ESA Special Publication, Vol. 560, 13th Cambridge Workshop on Cool Stars, Stellar Systems and the Sun, ed. F. Favata, G. A. J. Hussain, & B. Battrick, 571
Grether, D., & Lineweaver, C. H. 2006, ApJ, 640, 1051
Guillout, P., Klutsch, A., Frasca, A., et al. 2009, A&A, 504, 829
Hayano, Y., Takami, H., Guyon, O., et al. 2008, in Society of Photo-Optical Instrumentation Engineers (SPIE) Conference Series, Vol. 7015, Society of Photo-Optical Instrumentation Engineers (SPIE) Conference Series
Hayashi, C. 1981, Progress of Theoretical Physics Supplement, 70, 35
Hinkley, S., Pueyo, L., Faherty, J. K., et al. 2013, ApJ, 779, 153
Holman, M. J., & Wiegert, P. A. 1999, AJ, 117, 621
Hubickyj, O., Bodenheimer, P., & Lissauer, J. J. 2005, Icarus, 179, 415
Janson, M., Brandt, T. D., Kuzuhara, M., et al. 2013a, ApJ, 778, L4
Janson, M., Brandt, T. D., Moro-Martin, A., et al. 2013b, ArXiv e-prints, 1306.0581
Janson, M., Carson, J., Thalmann, C., et al. 2011, ApJ, 728, 85
Janson, M., Carson, J. C., Lafrenière, D., et al. 2012, ApJ, 747, 116
Johnson, J. A., Butler, R. P., Marcy, G. W., et al. 2007a, ApJ, 670, 833
Johnson, J. A., Fischer, D. A., Marcy, G. W., et al. 2007b, ApJ, 665, 785
Jurić, M., & Tremaine, S. 2008, ApJ, 686, 603
Kalas, P., Graham, J. R., Chiang, E., et al. 2008, Science, 322, 1345
Kenyon, S. J., & Bromley, B. C. 2009, ApJ, 690, L140
Kiraga, M. 2012, Acta Astron., 62, 67
Kirkpatrick, J. D., Gelino, C. R., Cushing, M. C., et al. 2012, ApJ, 753, 156
Kiss, L. L., Moór, A., Szalai, T., et al. 2011, MNRAS, 411, 117
Koen, C., & Eyer, L. 2002, MNRAS, 331, 45
Konopacky, Q. M., Barman, T. S., Macintosh, B. A., & Marois, C. 2013, Science, 339, 1398
Kratter, K. M., Murray-Clay, R. A., & Youdin, A. N. 2010, ApJ, 710, 1375
Kraus, A. L., & Ireland, M. J. 2012, ApJ, 745, 5
Kroupa, P. 2001, MNRAS, 322, 231

Kuiper, G. P. 1951, Proceedings of the National Academy of Science, 37, 1
Kuzuhara, M., Tamura, M., Kudo, T., et al. 2013, ApJ, 774, 11
Lafrenière, D., Doyon, R., Marois, C., et al. 2007, ApJ, 670, 1367
Lagrange, A.-M., De Bondt, K., Meunier, N., et al. 2012, A&A, 542, A18
Lagrange, A.-M., Gratadour, D., Chauvin, G., et al. 2009, A&A, 493, L21
Lambrechts, M., & Johansen, A. 2012, A&A, 544, A32
Lockwood, G. W., Skiff, B. A., Henry, G. W., et al. 2007, ApJS, 171, 260
López-Santiago, J., Montes, D., Crespo-Chacón, I., & Fernández-Figueroa, M. J. 2006, ApJ, 643, 1160
López-Santiago, J., Montes, D., Gálvez-Ortiz, M. C., et al. 2010, A&A, 514, A97
Low, C., & Lynden-Bell, D. 1976, MNRAS, 176, 367
Lowrance, P. J., Schneider, G., Kirkpatrick, J. D., et al. 2000, ApJ, 541, 390
Macintosh, B. A., Graham, J. R., Palmer, D. W., et al. 2008, in Society of Photo-Optical Instrumentation Engineers (SPIE) Conference Series, Vol. 7015, Society of Photo-Optical Instrumentation Engineers (SPIE) Conference Series
Malo, L., Doyon, R., Lafrenière, D., et al. 2013, ApJ, 762, 88
Mamajek, E. E., & Hillenbrand, L. A. 2008, ApJ, 687, 1264
Marcy, G. W., & Butler, R. P. 2000, PASP, 112, 137
Marcy, G. W., Butler, R. P., Fischer, D., et al. 2001, ApJ, 556, 296
Marcy, G. W., Butler, R. P., Vogt, S. S., Fischer, D., & Lissauer, J. J. 1998, ApJ, 505, L147
Marleau, G.-D., & Cumming, A. 2014, MNRAS, 437, 1378
Marley, M. S., Fortney, J. J., Hubickyj, O., Bodenheimer, P., & Lissauer, J. J. 2007, ApJ, 655, 541
Marois, C., Macintosh, B., Barman, T., et al. 2008, Science, 322, 1348
Marois, C., Zuckerman, B., Konopacky, Q. M., Macintosh, B., & Barman, T. 2010, Nature, 468, 1080
Mayor, M., & Queloz, D. 1995, Nature, 378, 355
McCarthy, K., & White, R. J. 2012, AJ, 143, 134
Merín, B., Montesinos, B., Eiroa, C., et al. 2004, A&A, 419, 301
Messina, S., Desidera, S., Lanzafame, A. C., Turatto, M., & Guinan, E. F. 2011, A&A, 532, A10
Messina, S., Desidera, S., Turatto, M., Lanzafame, A. C., & Guinan, E. F. 2010, A&A, 520, A15
Messina, S., & Guinan, E. F. 1996, Information Bulletin on Variable Stars, 4286, 1
Messina, S., Pizzolato, N., Guinan, E. F., & Rodonò, M. 2003, A&A, 410, 671
Metchev, S. A., & Hillenbrand, L. A. 2009, ApJS, 181, 62
Mishenina, T. V., Soubiran, C., Bienaymé, O., et al. 2008, A&A, 489, 923
Mishenina, T. V., Soubiran, C., Kovtyukh, V. V., Katsova, M. M., & Livshits, M. A. 2012, A&A, 547, A106
Moór, A., Pascucci, I., Kóspál, Á., et al. 2011, ApJS, 193, 4
Moór, A., Szabó, G. M., Kiss, L. L., et al. 2013, MNRAS, 435, 1376
Mordasini, C. 2013, A&A, 558, A113
Munari, U., Dallaporta, S., Siviero, A., et al. 2004, A&A, 418, L31
Nielsen, E. L., & Close, L. M. 2010, ApJ, 717, 878
Nielsen, E. L., Liu, M. C., Wahhaj, Z., et al. 2012, ApJ, 750, 53
Nielsen, E. L., Liu, M. C., Wahhaj, Z., et al. 2013, ArXiv e-prints, 1306.1233
Norton, A. J., Wheatley, P. J., West, R. G., et al. 2007, A&A, 467, 785
Pace, G. 2013, A&A, 551, L8
Pecaut, M. J., Mamajek, E. E., & Bubar, E. J. 2012, ApJ, 746, 154
Peters, M. A., Groff, T., Kasdin, N. J., et al. 2012, in Society of Photo-Optical Instrumentation Engineers (SPIE) Conference Series, Vol. 8446, Society of Photo-Optical Instrumentation Engineers (SPIE) Conference Series
Plavchan, P., Werner, M. W., Chen, C. H., et al. 2009, ApJ, 698, 1068
Pojmanski, G., Pilecki, B., & Szczygiel, D. 2005, Acta Astron., 55, 275
Pollacco, D. L., Skillen, I., Collier Cameron, A., et al. 2006, PASP, 118, 1407
Pollack, J. B., Hubickyj, O., Bodenheimer, P., et al. 1996, Icarus, 124, 62
Radick, R. R., Lockwood, G. W., Skiff, B. A., & Baliunas, S. L. 1998, ApJS, 118, 239
Rafikov, R. R. 2005, ApJ, 621, L69
Raghavan, D., McAlister, H. A., Henry, T. J., et al. 2010, ApJS, 190, 1
Rameau, J., Chauvin, G., Lagrange, A.-M., et al. 2013, ApJ, 772, L15
Reid, I. N., Gizis, J. E., & Hawley, S. L. 2002, AJ, 124, 2721
Rieke, G. H., Su, K. Y. L., Stansberry, J. A., et al. 2005, ApJ, 620, 1010
Rivera, E. J., Laughlin, G., Butler, R. P., et al. 2010, ApJ, 719, 890
Rivera, E. J., Lissauer, J. J., Butler, R. P., et al. 2005, ApJ, 634, 625
Rodriguez, D. R., Marois, C., Zuckerman, B., Macintosh, B., & Melis, C. 2012, ApJ, 748, 30
Rodriguez, D. R., Zuckerman, B., Kastner, J. H., et al. 2013, ApJ, 774, 101
Salpeter, E. E. 1955, ApJ, 121, 161
Samus, N. N., Durlevich, O. V., & et al. 2009, VizieR Online Data Catalog, 1, 2025
Schlieder, J. E., Lépine, S., & Simon, M. 2010, AJ, 140, 119
Schlieder, J. E., Lépine, S., & Simon, M. 2012, AJ, 143, 80
Shkolnik, E. L., Anglada-Escudé, G., Liu, M. C., et al. 2012, ApJ, 758, 56
Soderblom, D. R. 2010, ARA&A, 48, 581
Song, I., Zuckerman, B., & Bessell, M. S. 2012, AJ, 144, 8
Spiegel, D. S., & Burrows, A. 2012, ApJ, 745, 174
Spiegel, D. S., Burrows, A., & Milsom, J. A. 2011, ApJ, 727, 57
Stamatellos, D., & Whitworth, A. P. 2009, MNRAS, 392, 413
Stauffer, J. R., Schultz, G., & Kirkpatrick, J. D. 1998, ApJ, 499, L199
Sudol, J. J., & Haghighipour, N. 2012, ApJ, 755, 38
Sumi, T., Kamiya, K., Bennett, D. P., et al. 2011, Nature, 473, 349
Suzuki, R., Kudo, T., Hashimoto, J., et al. 2010, Proc. SPIE, 7735
Takeda, Y., & Kawanomoto, S. 2005, PASJ, 57, 45
Tamura, M. 2009, in American Institute of Physics Conference Series, Vol. 1158, American Institute of Physics Conference Series, ed. T. Usuda, M. Tamura, & M. Ishii, 11
Thalmann, C., Carson, J., Janson, M., et al. 2009, ApJ, 707, L123
Thies, I., & Kroupa, P. 2007, ApJ, 671, 767
Thies, I., & Kroupa, P. 2008, MNRAS, 390, 1200
Torres, C. A. O., Quast, G. R., da Silva, L., et al. 2006, A&A, 460, 695
Torres, C. A. O., Quast, G. R., Melo, C. H. F., & Sterzik, M. F. 2008, Young Nearby Loose Associations, ed. B. Reipurth 757
Umbreit, S., Burkert, A., Henning, T., Mikkola, S., & Spurzem, R. 2005, ApJ, 623, 940
van Leeuwen, F. 2009, A&A, 497, 209
Vigan, A., Patience, J., Marois, C., et al. 2012, A&A, 544, A9
Vorobyov, E. I. 2013, A&A, 552, A129
Wahhaj, Z., Liu, M. C., Biller, B. A., et al. 2011, ApJ, 729, 139
Wahhaj, Z., Liu, M. C., Biller, B. A., et al. 2013a, ApJ, 779, 80
Wahhaj, Z., Liu, M. C., Nielsen, E. L., et al. 2013b, ApJ, 773, 179
White, R. J., Gabor, J. M., & Hillenbrand, L. A. 2007, AJ, 133, 2524
Whitworth, A. P., & Stamatellos, D. 2006, A&A, 458, 817
Wright, N. J., Drake, J. J., Mamajek, E. E., & Henry, G. W. 2011, ApJ, 743, 48
Yamamoto, K., Matsuo, T., Shibai, H., et al. 2013, ArXiv e-prints, 1306.3100
Zuckerman, B., Rhee, J. H., Song, I., & Bessell, M. S. 2011, ApJ, 732, 61
Zuckerman, B., & Song, I. 2004, ARA&A, 42, 685
Zuckerman, B., & Song, I. 2009, A&A, 493, 1149
Zuckerman, B., & Song, I. 2012, ApJ, 758, 77
Zuckerman, B., Song, I., Bessell, M. S., & Webb, R. A. 2001, ApJ, 562, L87
Zuckerman, B., & Webb, R. A. 2000, ApJ, 535, 959